Figure 1. Temperature Programmed Reduction of the UCI unsupported catalyst in CO. Peaks corresponding to reduction of CuO --> Cu metal, hematite --> magnetite and magnetite --> α-Fe are seen. Peak identification is based on TEM analysis of samples withdrawn at various stages as well as from x-ray diffraction

Fig. 2 CO TPR of the UCI unsupported catalyst. After the first run, the sample was oxidized and a second TPR was run. TEM analysis was performed as indicated by arrows. These TEM images are presented in the following figures.

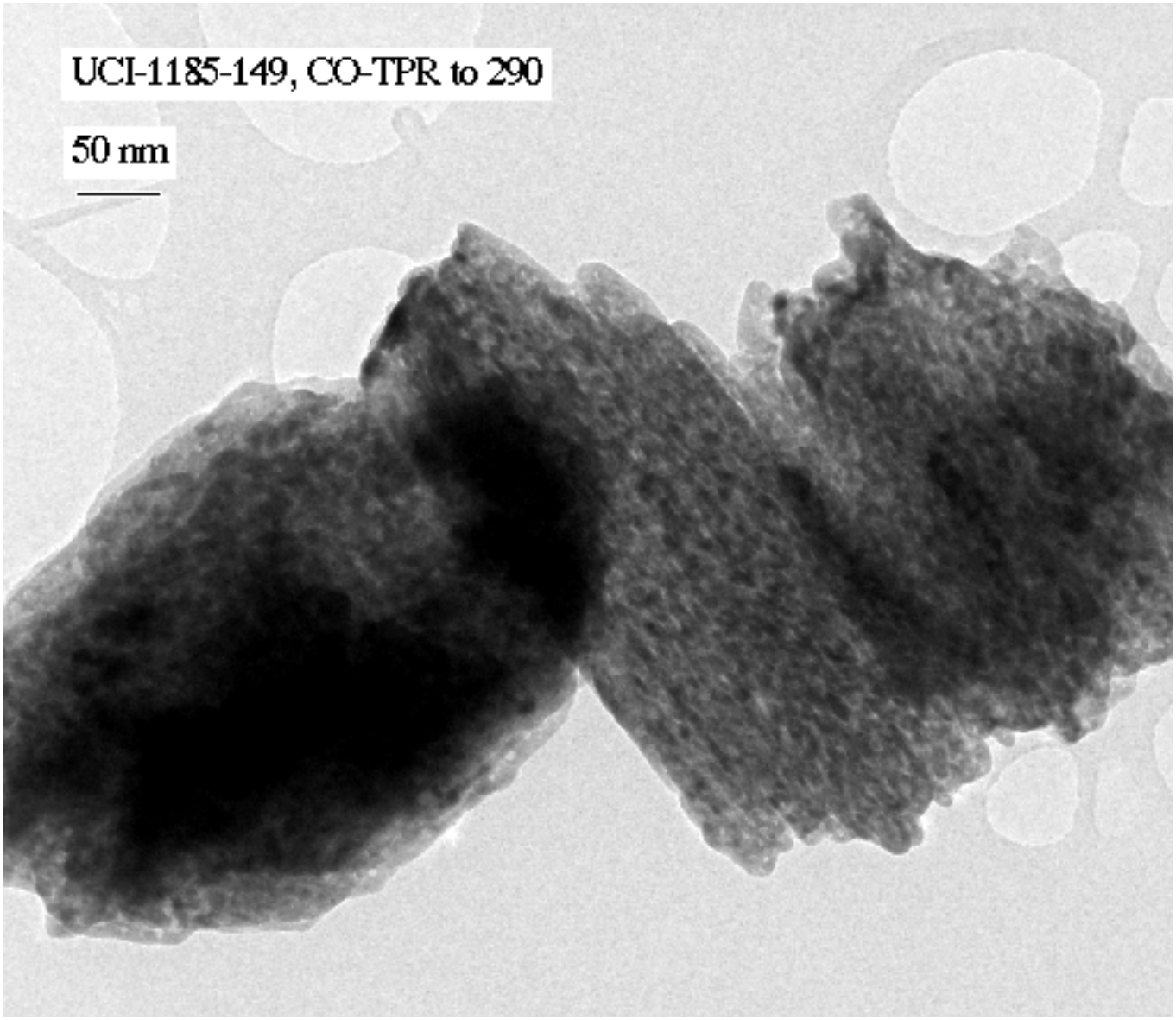

Figure 3a Low magnification view of UCI unsupported catalyst after CO TPR up to 290 °C. The "Swiss-cheese" morphology of the hematite catalyst is preserved, however the catalyst has completely transformed into magnetite

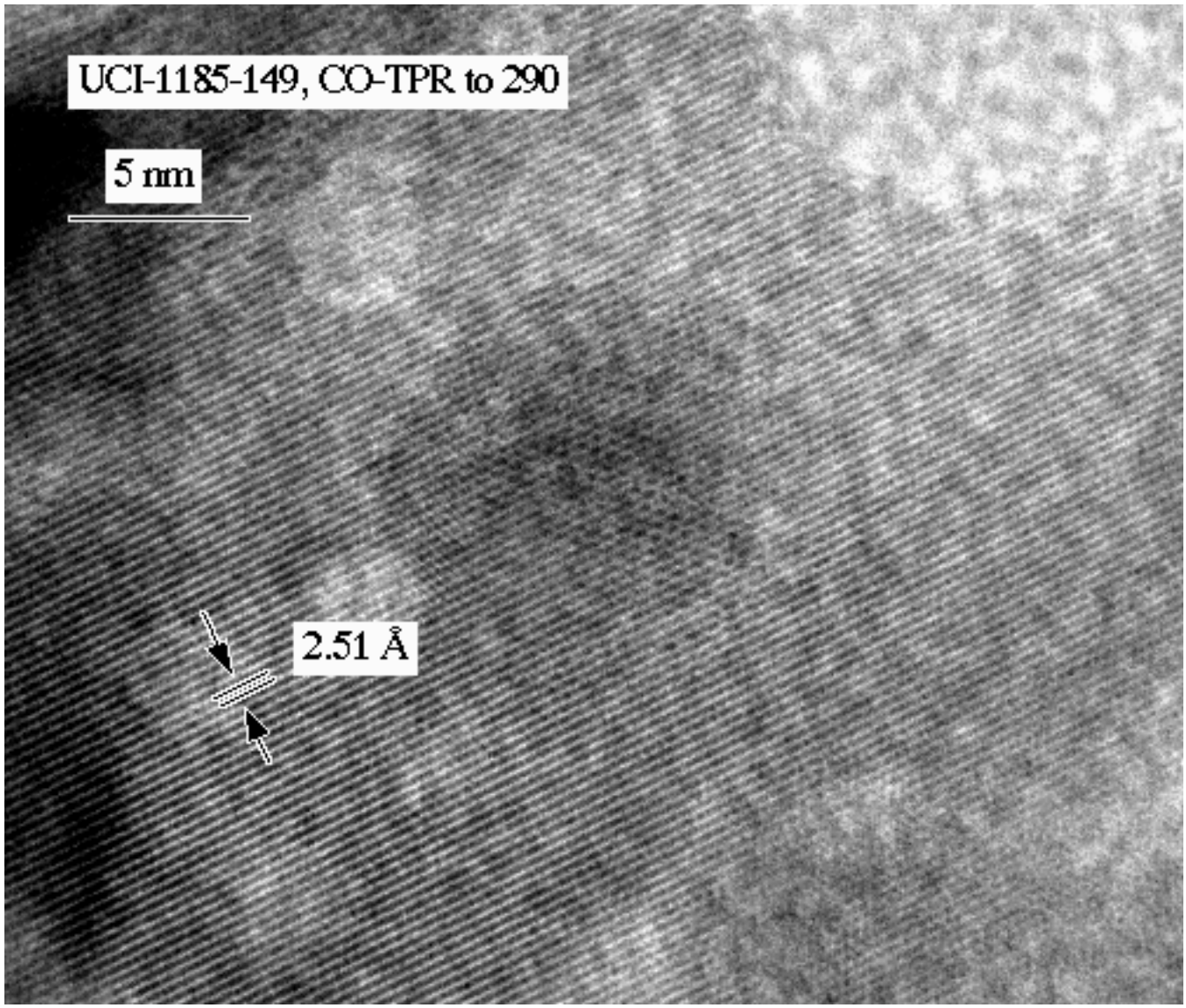

Fig. 3b Higher magnification view of the catalyst shown in Fig. 3a. Lattice fringes corresponding to magnetite can be clearly seen. The individual particles are single crystals.

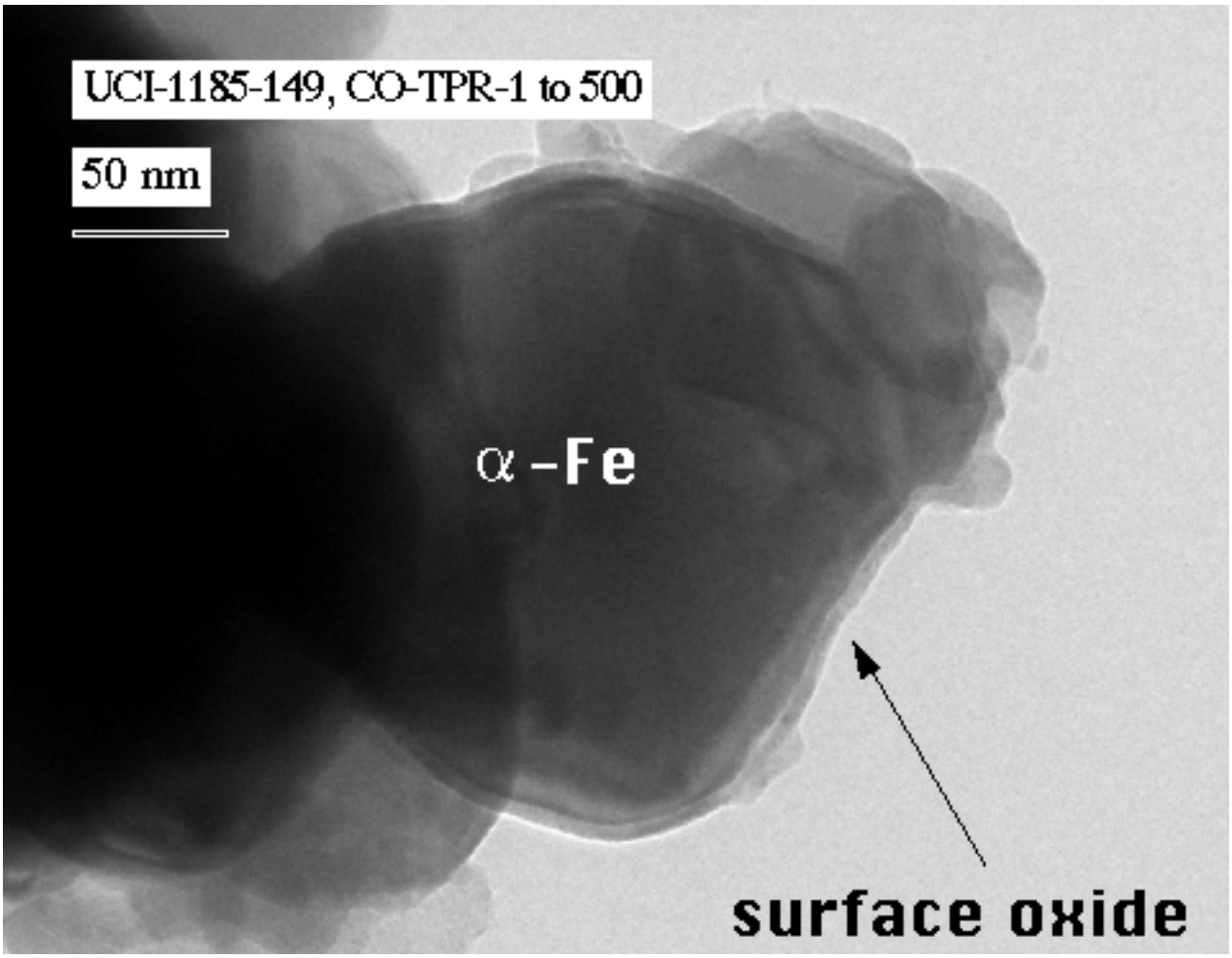

Fig. 4a Low magnification view of UCI catalyst after CO TPR to 500 °C. Large metallic particles of α-Fe are seen. The surface oxide is caused by exposure to air during transfer to the electron microscope. What is surprising is the absence of any amorphous carbon or graphite considering that the sample was reduced in CO at 500 °C.

Fig. 4b (on the next page) shows an electron diffraction pattern from this sample. The large Fe particles give rise to the diffraction spots while the surface oxide (magnetite) gives a diffuse ring pattern.

Fig. 4c (on the next page) shows a higher magnification view of the α-Fe crystals showing lattice fringes.

b

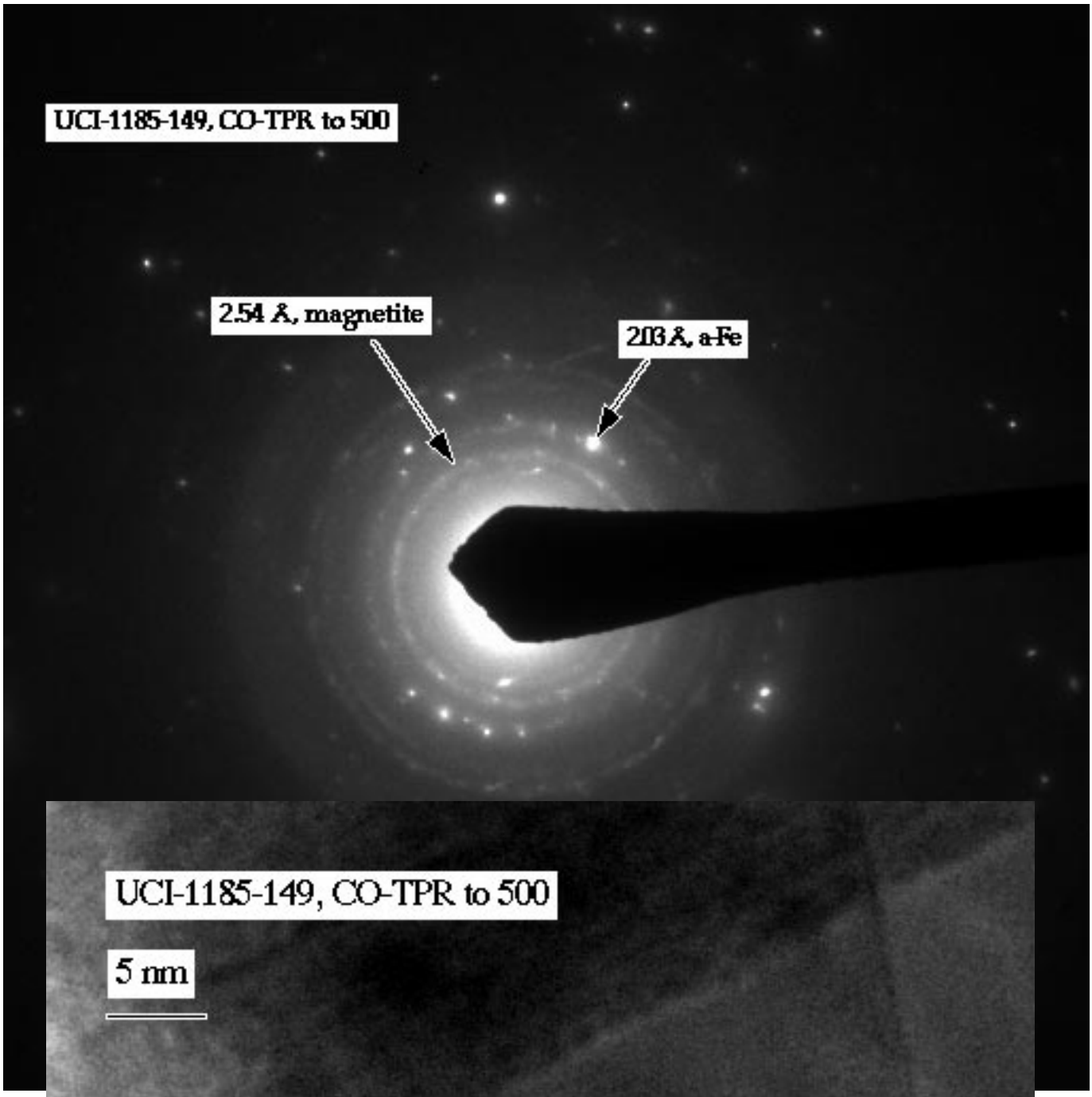
UCI-1185-149, CO-TPR to 500
2.54 Å, magnetite
2.03 Å, a-Fe

c

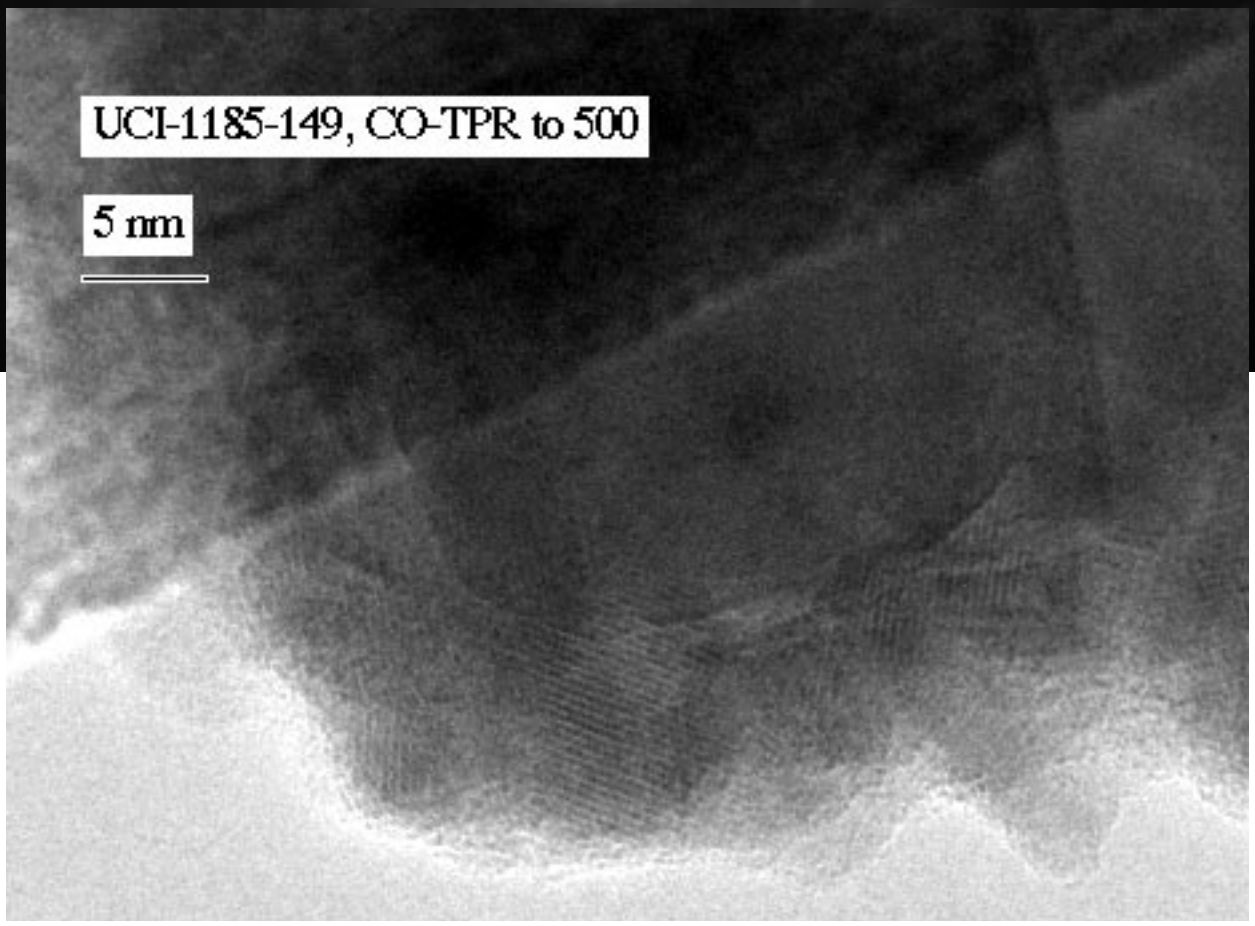
UCI-1185-149, CO-TPR to 500
5 nm

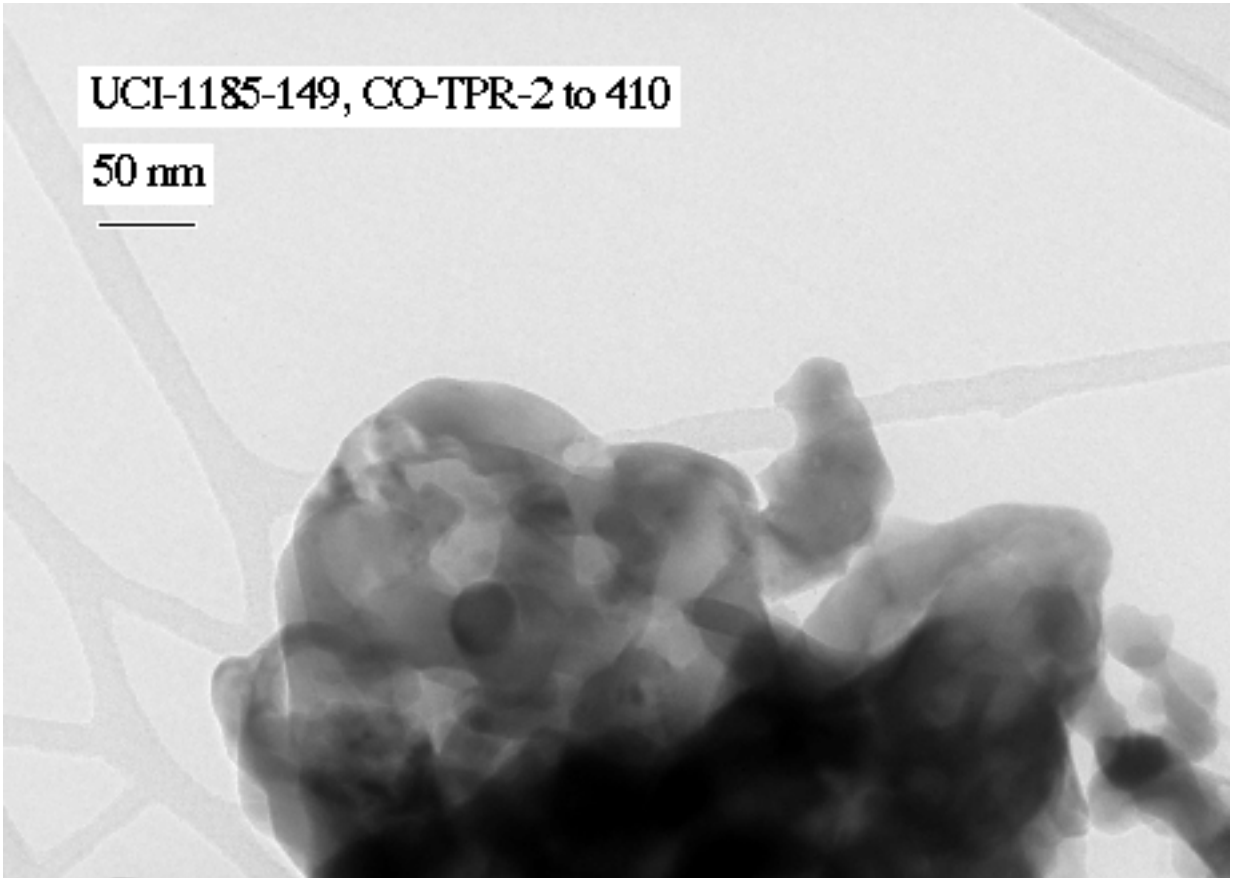

a

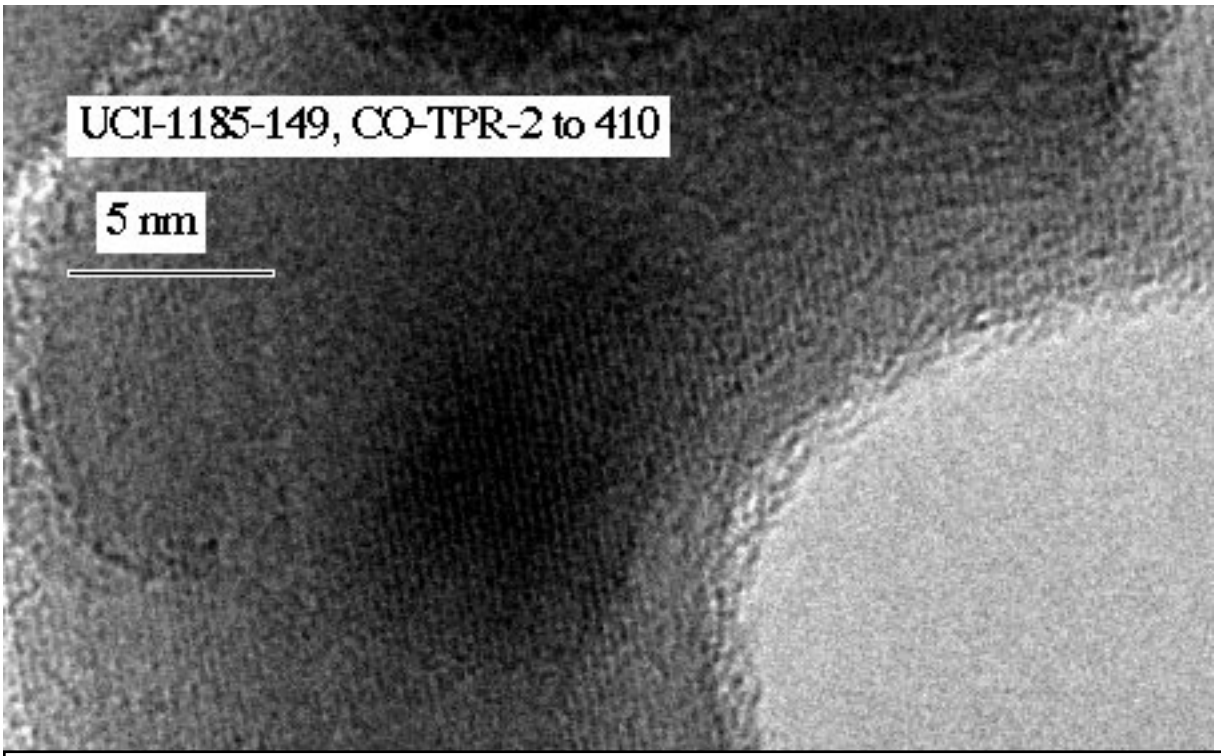

b

Figure 5 TEM of UCI catalyst during the 2nd TPR (i.e. after reduction in CO, oxidation at 500 °C). Low mag view (a) and Higher magnification view (b). Note the magnetite is much more dense than the one in Fig. 3 explaining the higher temperature required for reduction.

TEM pictures of unsupported UCI catalyst after CO-TPR

---transformation to α-Fe with a surface passivation layer,

---no carbide;sintering of metal particles

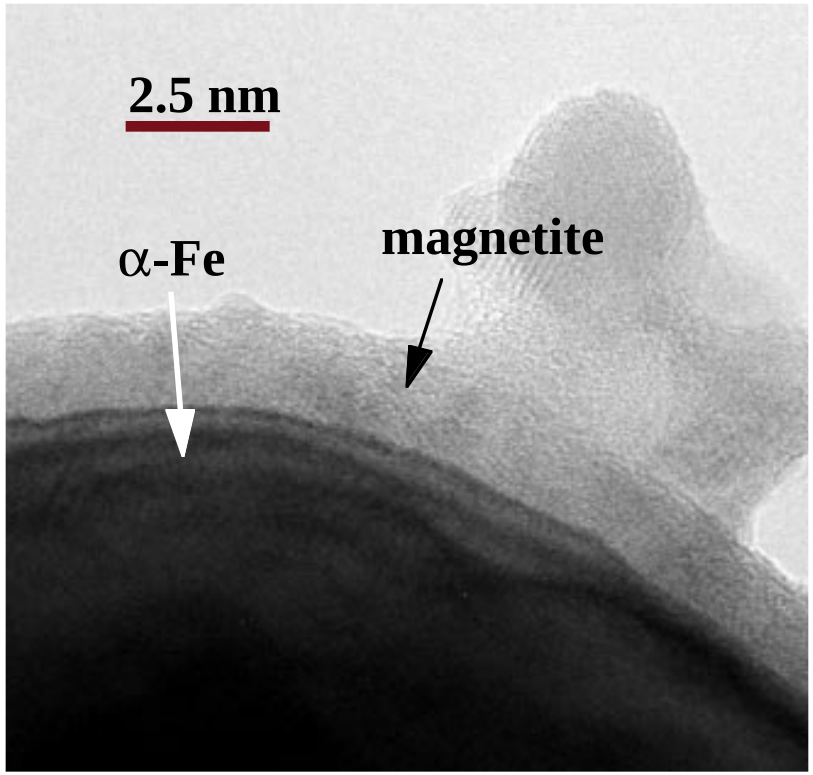

high mag. picture

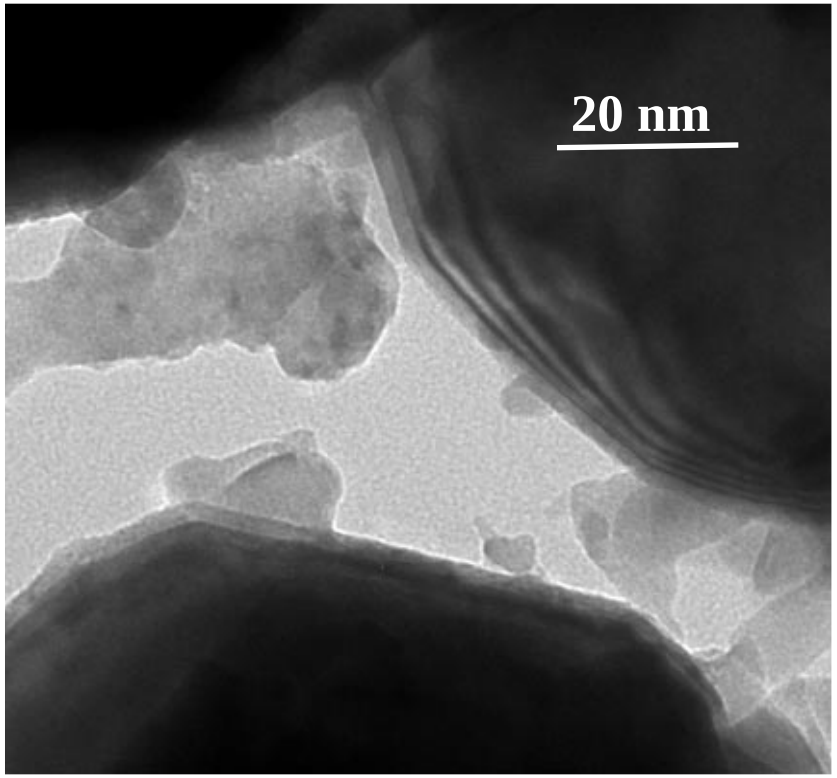

low mag. picture

Fig. 6 TEM after 2nd CO TPR of UCI unsupported catalyst. There is no evidence of any any carbonaceous species being present on the surface.

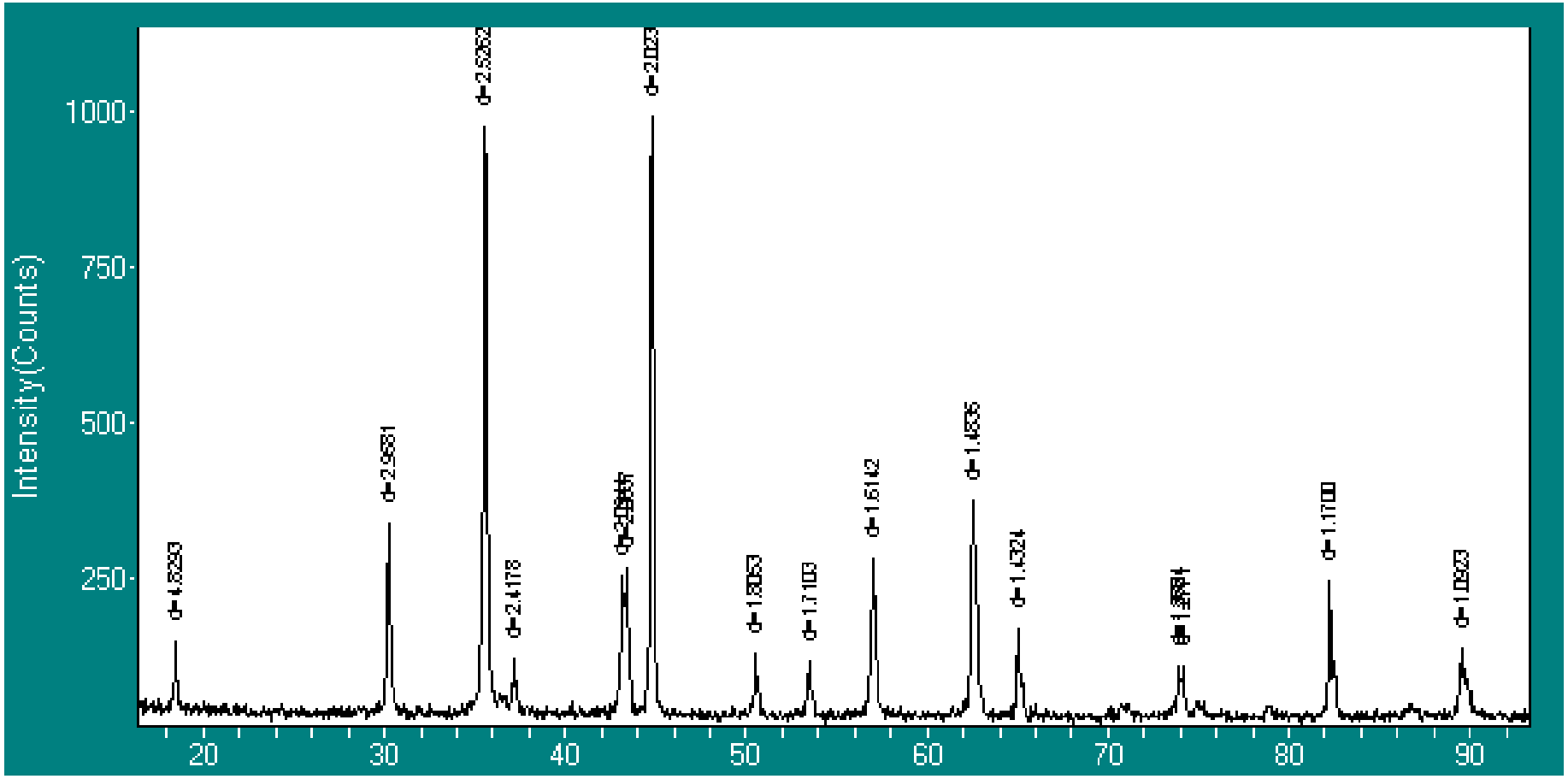

Fig. 7 X-ray diffraction pattern of the UCI catalyst after 2nd CO TPR. For this experiment, we used 0.120 g of sample instead of 0.020 g as in a typical TPR run. Hence the extent of reduction of the magnetite maybe somewhat less than in a conventional TPR experiment. Nonetheless, the xrd pattern shows clearly that under conditions of CO TPR where temperature is ramped at 10 °C/min, an unsupported Fe, Cu catalyst transforms into α-Fe instead of into iron carbide. This is in contrast to the behavior of a supported Fe, Cu catalyst shown in Figures 8-11 where it is seen that the catalyst directly transforms into iron carbide without an identifiable α-Fe transitional phase. We believe that the smaller particle size of the magnetite in the supported catalyst facilitates trasnformation into iron carbide.

Fig. 8 CO TPR of a supported Fe(Cu) catalyst. The catalyst support consists of microspheres of silica. Three peaks are seen, first hematite --> magnetite, second magnetite --> iron carbide and the third corresponding to the Boudouard reaction CO --> C(surface) + CO_2. Peak identification is based on TEM images shown in Fig. 9 and 10 and on the x-ray diffraction pattern in Fig. 11.

TEM picture of Fe(Cu)-supported after CO-TPR to 380°C

Diffuse spot diffraction pattern from iron carbide polycrstals

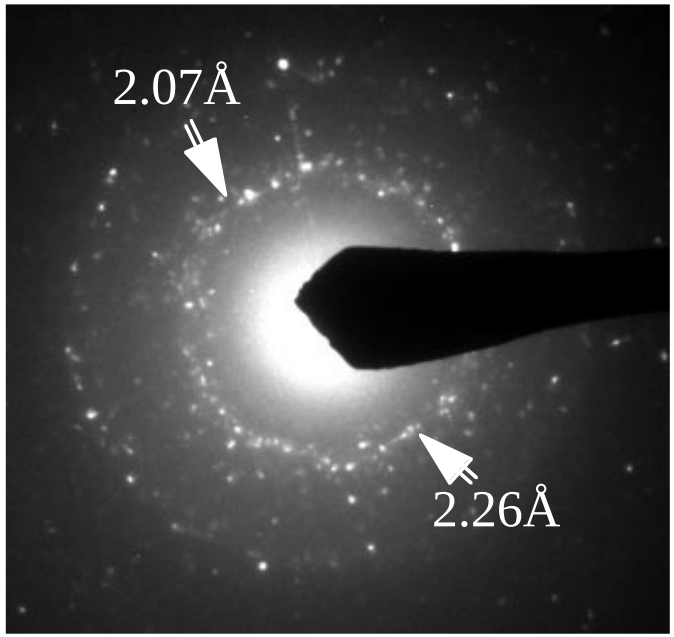

electron diffraction pattern

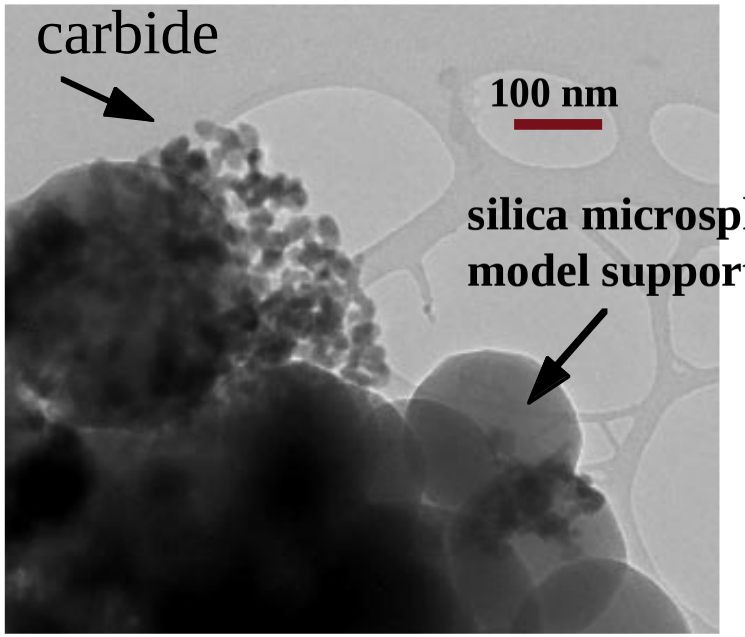

low mag. picture

Fig. 9a) Electron Diffraction pattern and b)Low magnification image of the Cu promoted, Fe catalyst. The model silica support makes it easier to study the morphology of the Fe catalyst. After CO TPR to 380 °C small crystals of iron carbide are seen. The carbide is identified from its electron diffraction pattern and the XRD pattern (Fig. 10) of this sample.

HRTEM of Fe(Cu)-supported catalyst CO-TPR to 380°C

Small iron carbide particles surrounded by a layer of amorphous carbon

No oxide layer because of carbon layer protection

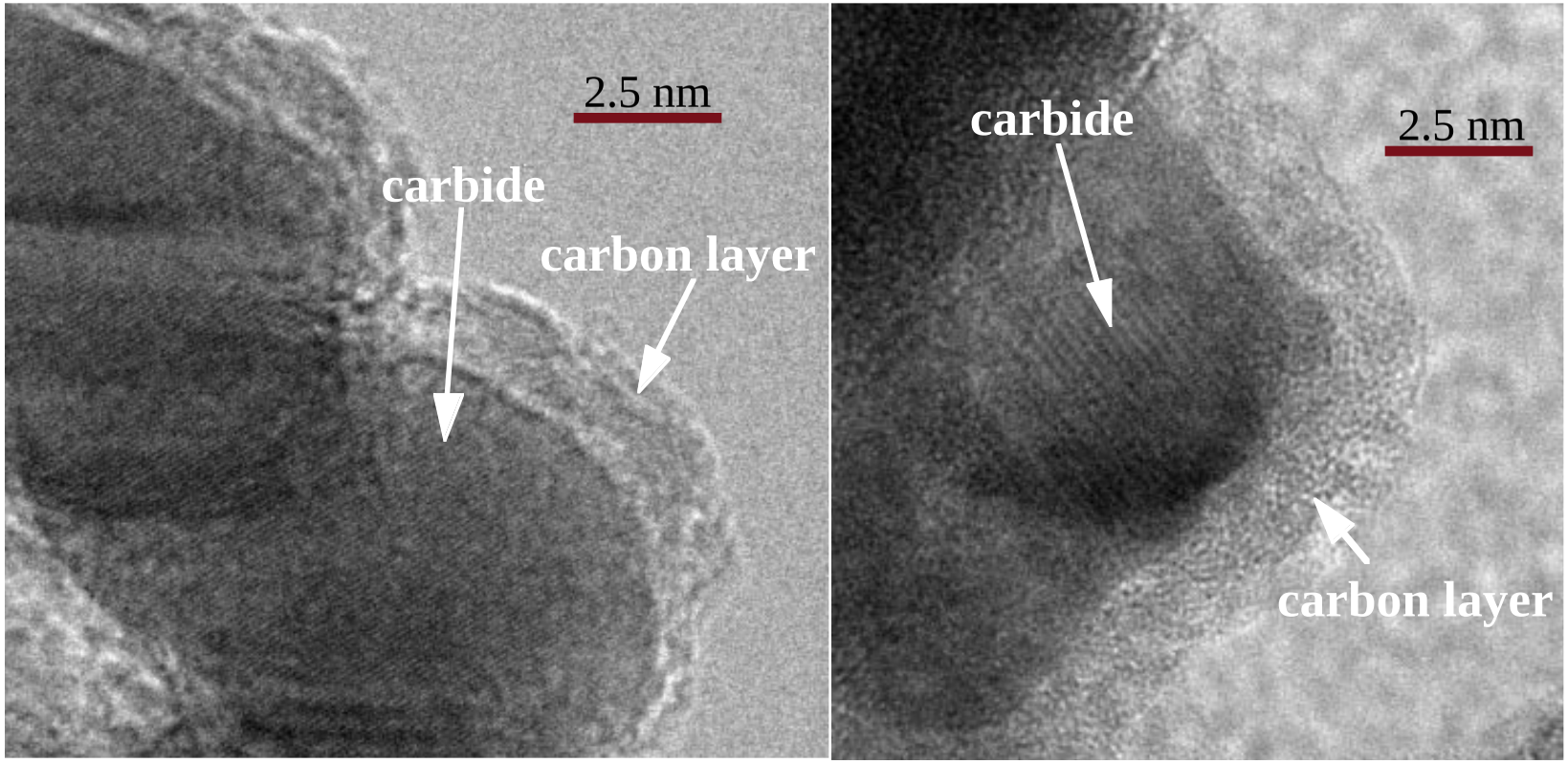

Fig. 9(contnued). c) and d) These are higher magnification views of the sample seen on the previous page. The carbide particles show amorphous carbon being present on the particle surface (in contrast to the α–Fe particles in Fig. 4 and 6) that show only a surface oxide being present. In this sample, the amorphous carbon prevents oxidation of the catalyst.

TEM picture of Fe(Cu)-supported after CO-TPR to 500 °C

3.32Å d-spacing coresponding to graphite, diffuse spots around 2Å from carbide

The higher temperature causes significant deposition of carbon, as graphite.

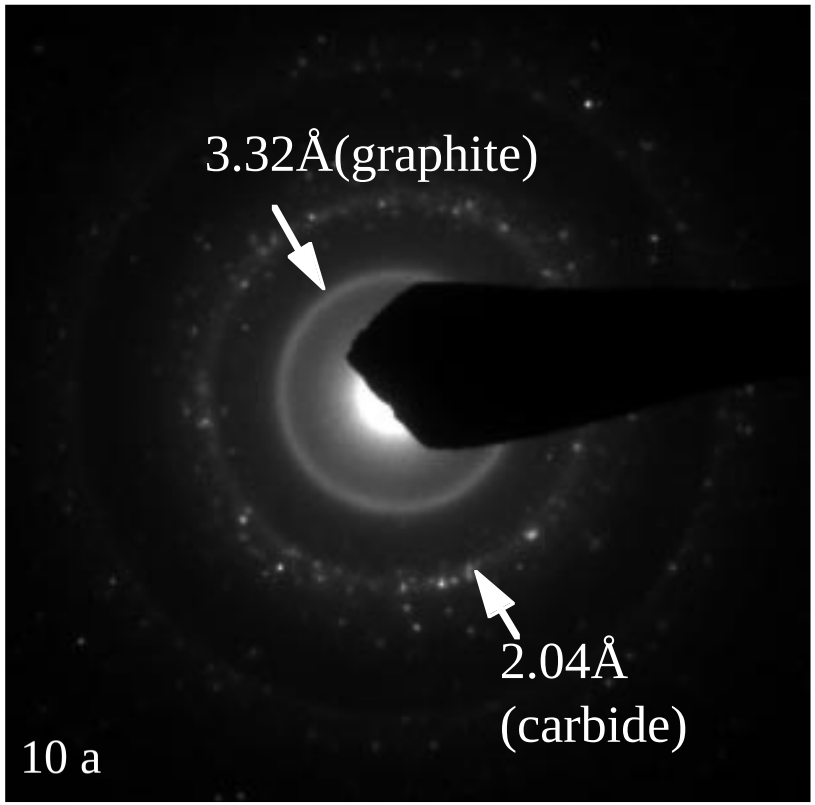

electron diffraction pattern

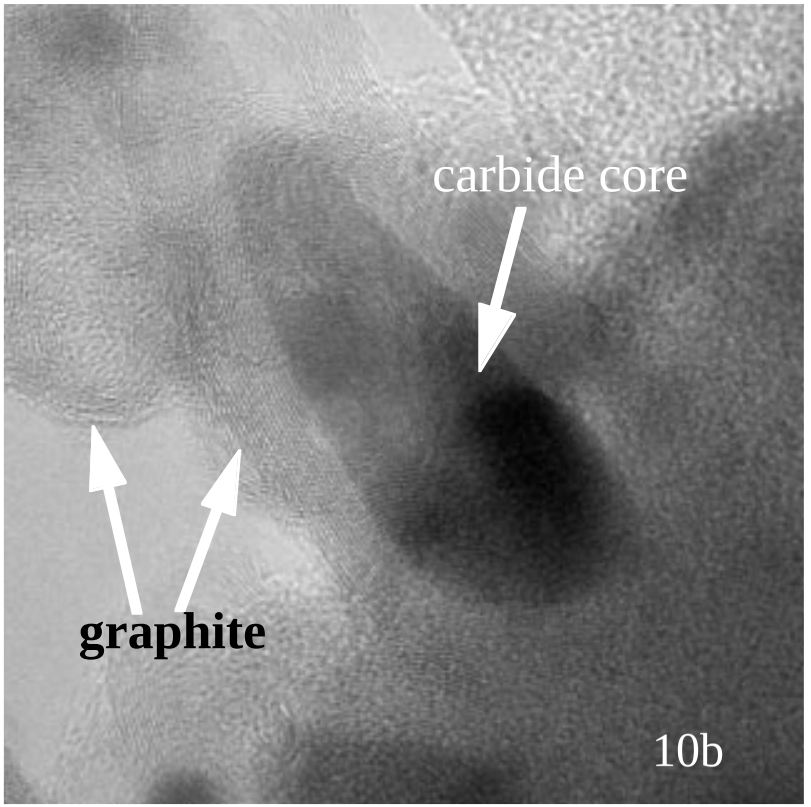

high mag. picture

TEM pictures of Fe(Cu)-supported catalyst after CO-TPR

A lot of carbon deposition and the carbon layer provides protection of underneath carbide against oxidation, no magnetite is observed

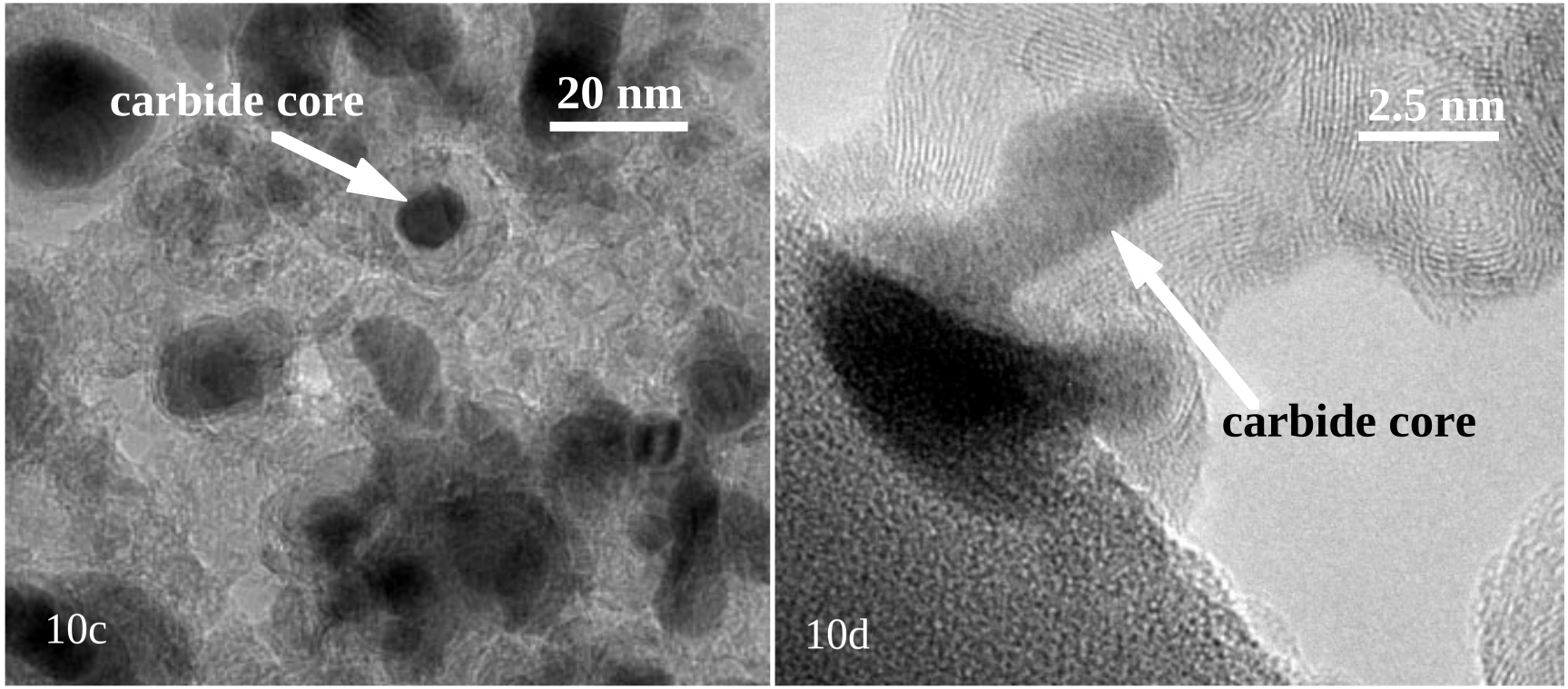

low mag. picture

high mag. picture

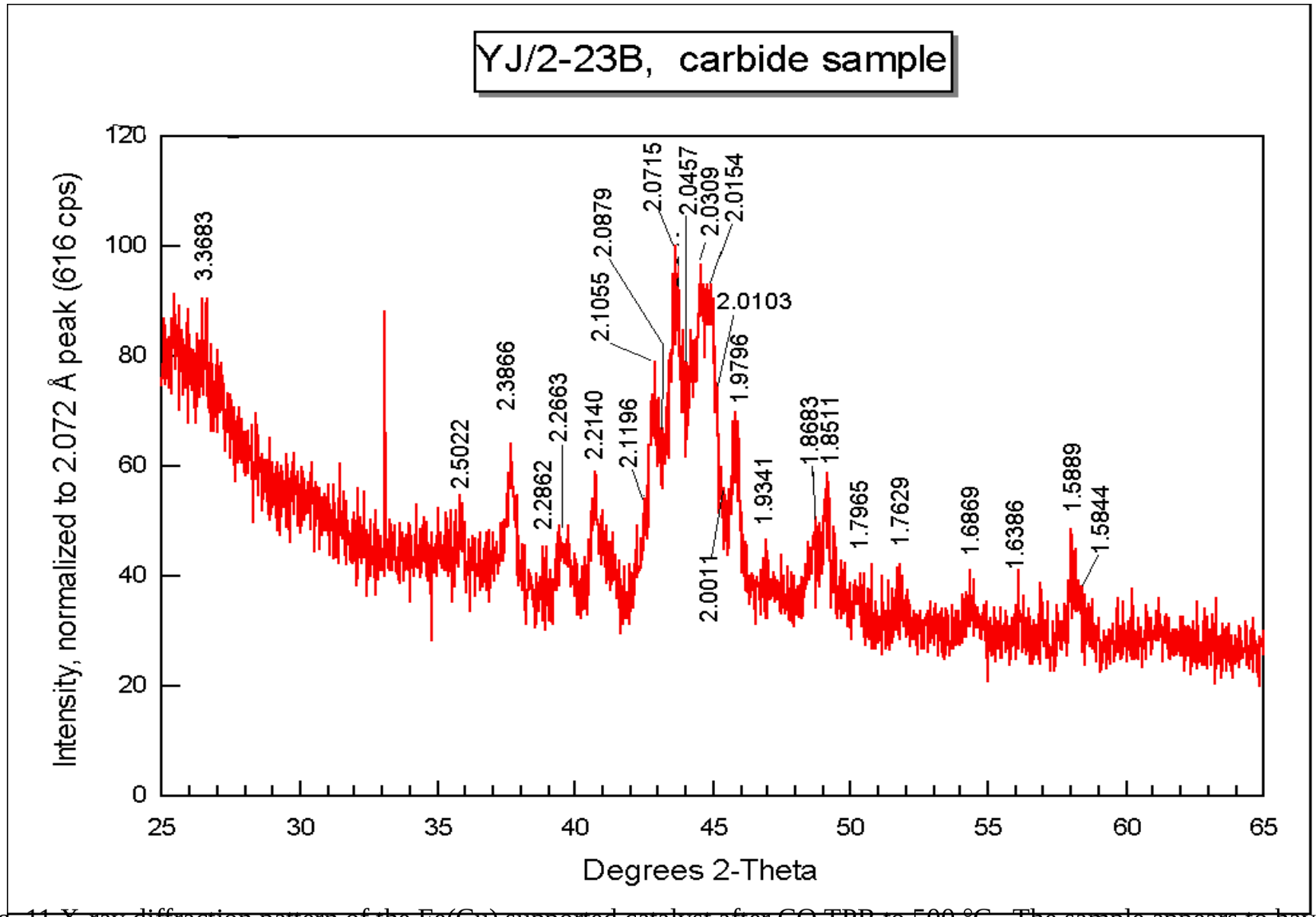

Fig. 11 X-ray diffraction pattern of the Fe(Cu) supported catalyst after CO TPR to 500 °C. The sample appears to have transformed completely to carbide. No magnetite is seen by XRD, which is consistent with the TEM images shown in Figures 9 and 10, where the carbonaceous layers on the surface helps protect the carbide from oxidation.

12 a

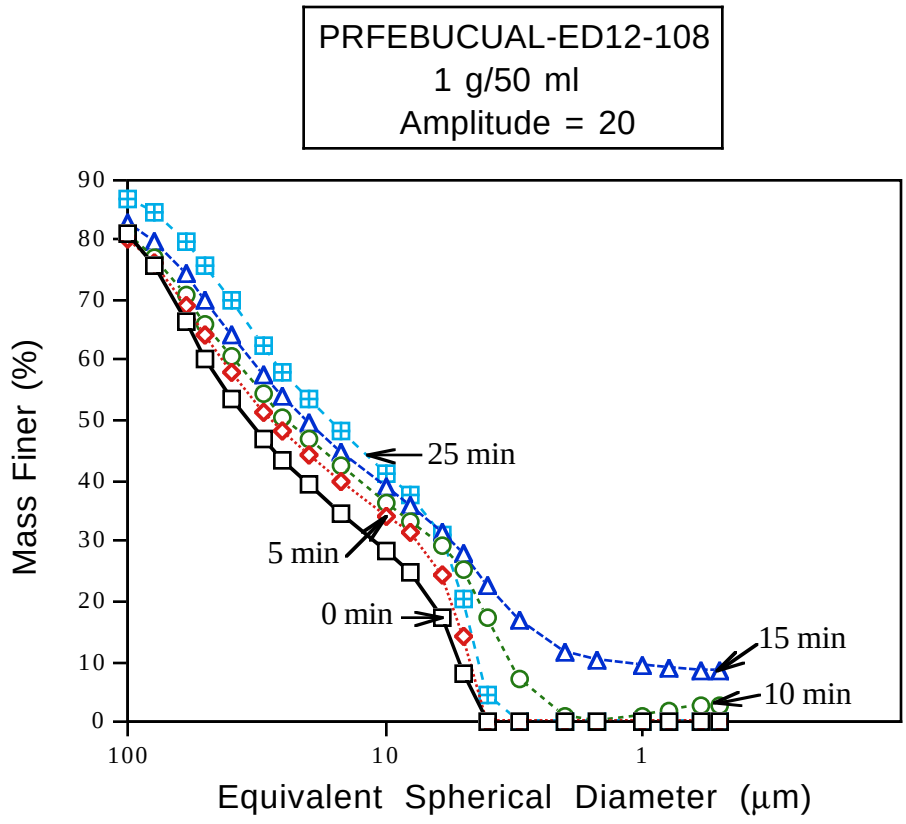

Fig. 12 Ultrasonic Fragmentation results for catalyst PRFECUBUAL-ED12-108 (12 a), PRFECUAL4K-ED12-112 (12 b, next page) and PRFECUPRAL/4K-ED11-117 (12c, next page) prepared by Robert Gormley, FETC. Samples 112 and 117 have had K added and had been calcined at 350 °C and appear comparable in strength to the uncalcined sample 108. These results suggest that calcination at this temperature does not result in a significant increase in agglomerate strength compared with the uncalcined sample.

12 b

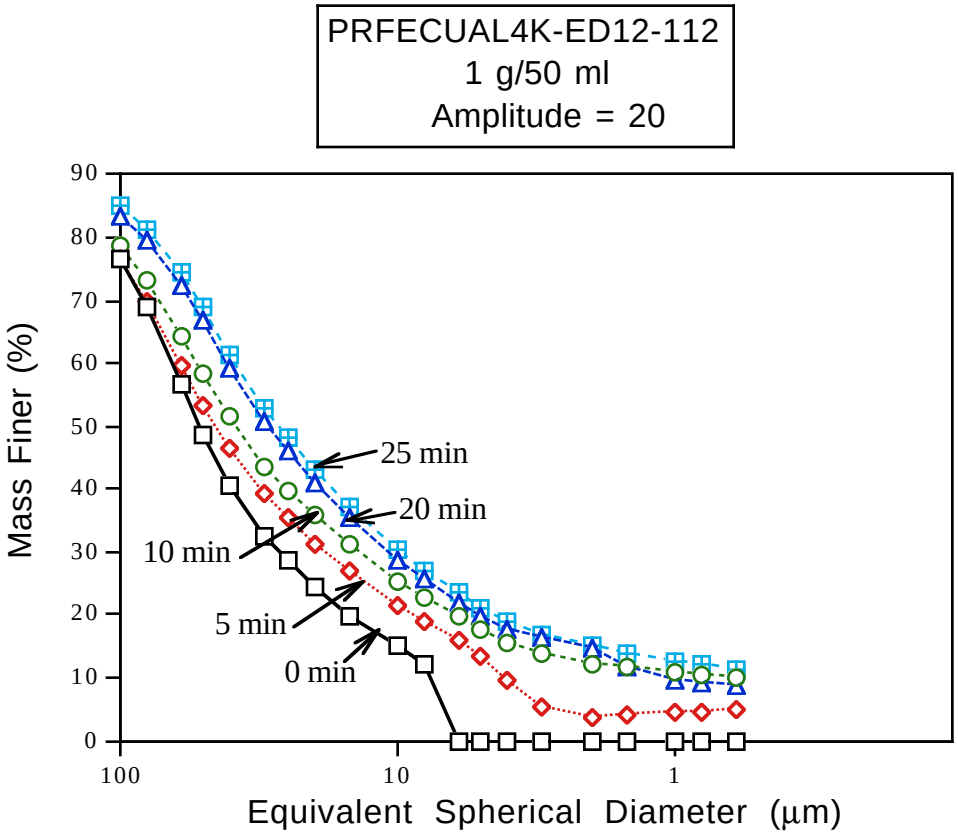
PRFECUAL4K-ED12-112
1 g/50 ml
Amplitude = 20
Mass Finer (%)
90
80
70
60
50
40
30
20
10
0
25 min
20 min
10 min
5 min
0 min
100
10
1
Equivalent Spherical Diameter (µm)

12 c

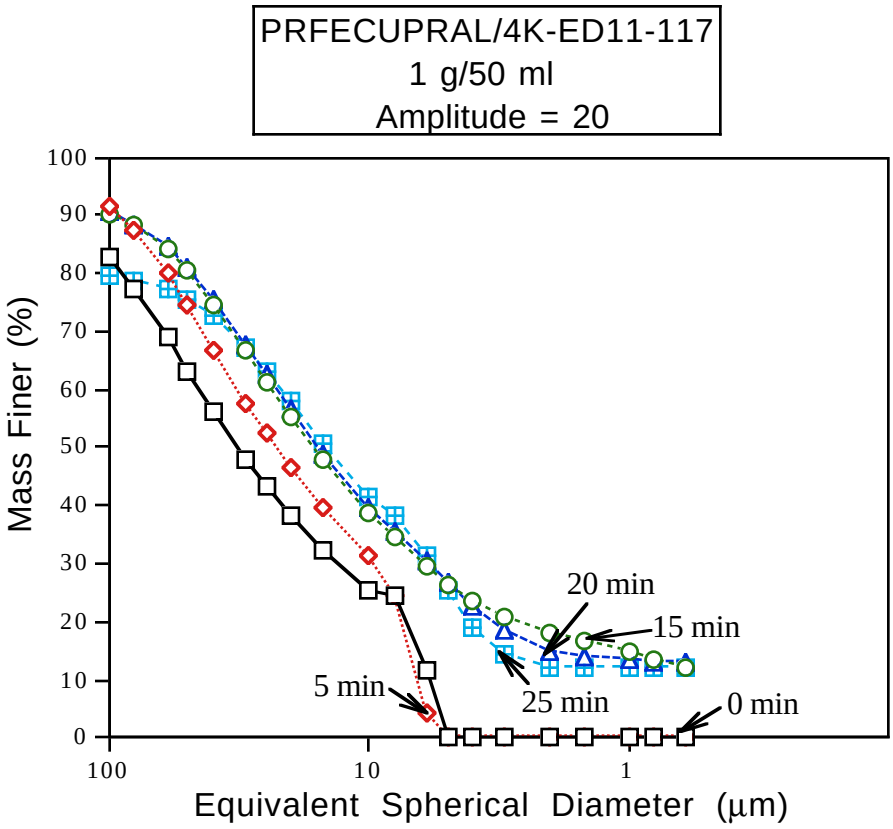
PRFECUPRAL/4K-ED11-117
1 g/50 ml
Amplitude = 20
Mass Finer (%)
100
90
80
70
60
50
40
30
20
10
0
20 min
15 min
5 min
25 min
0 min
100
10
1
Equivalent Spherical Diameter (µm)

13 a

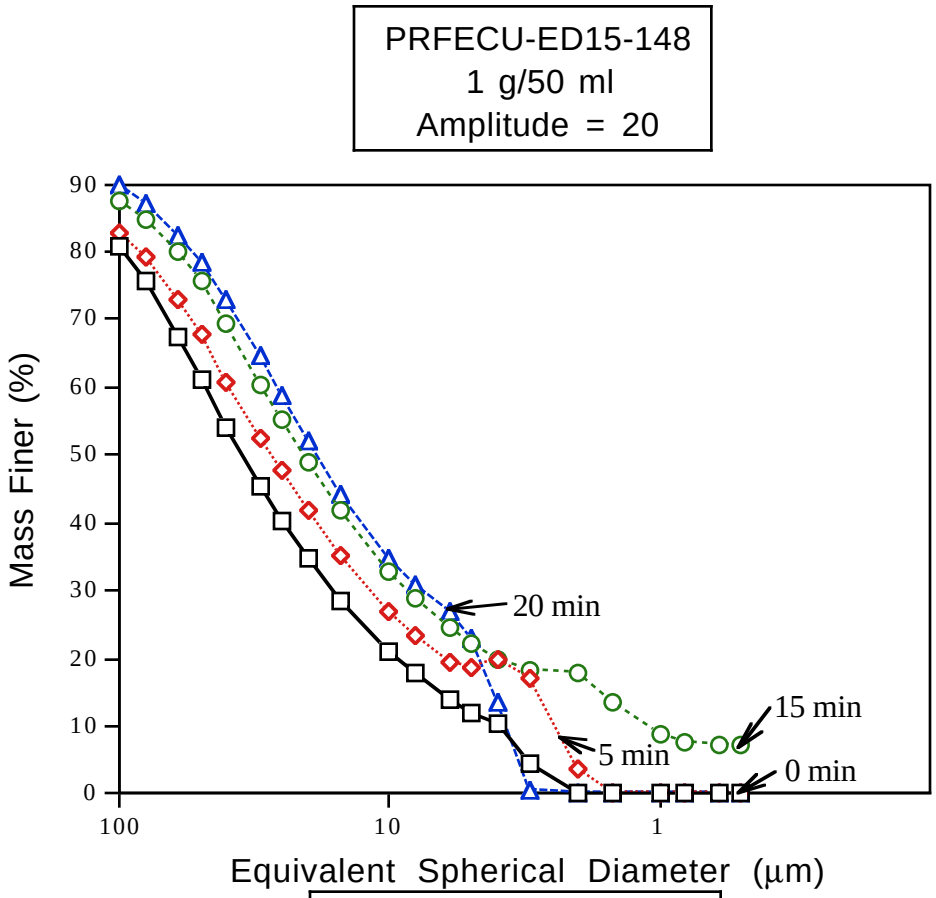

13 b

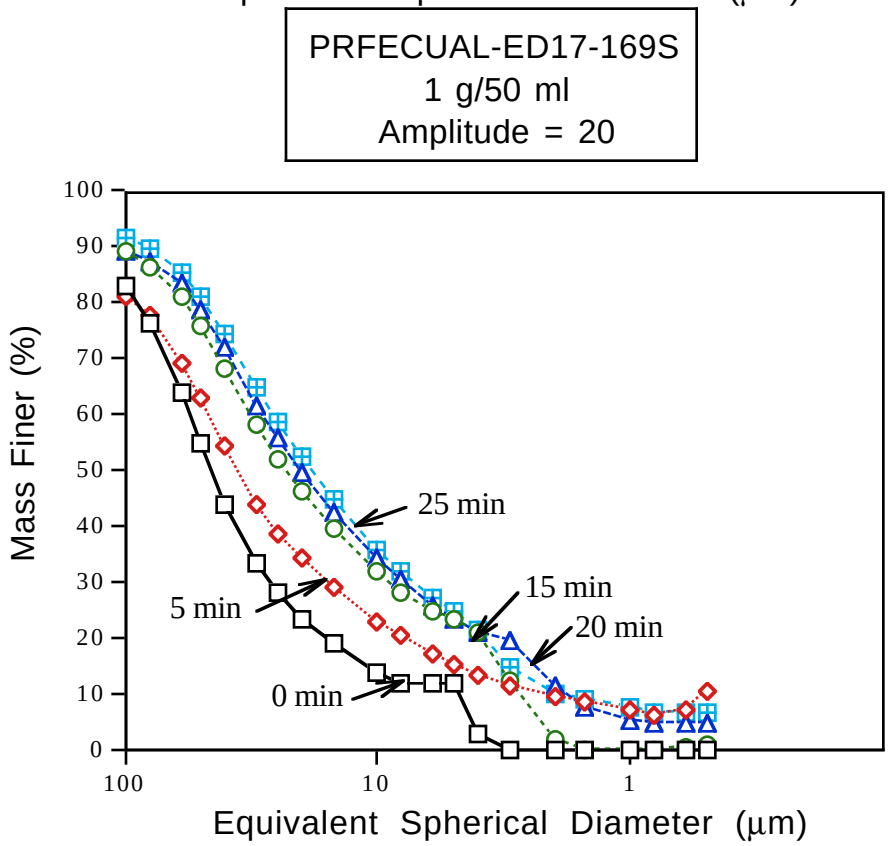

Fig. 13 Ultrasonic fragmentation results for a precipitated Fe catalysts prepared by Robert Gormley at FETC. Fig. 13 a shows a co-precipitated Fe-Cu oxide catalyst, while 13 b represents a co-precipitated Fe-Cu-Al oxide catalyst with the -400 mesh fines removed. Both had no K added and were uncalcined. The alumina does not appear to impart any additional strength to the powder.

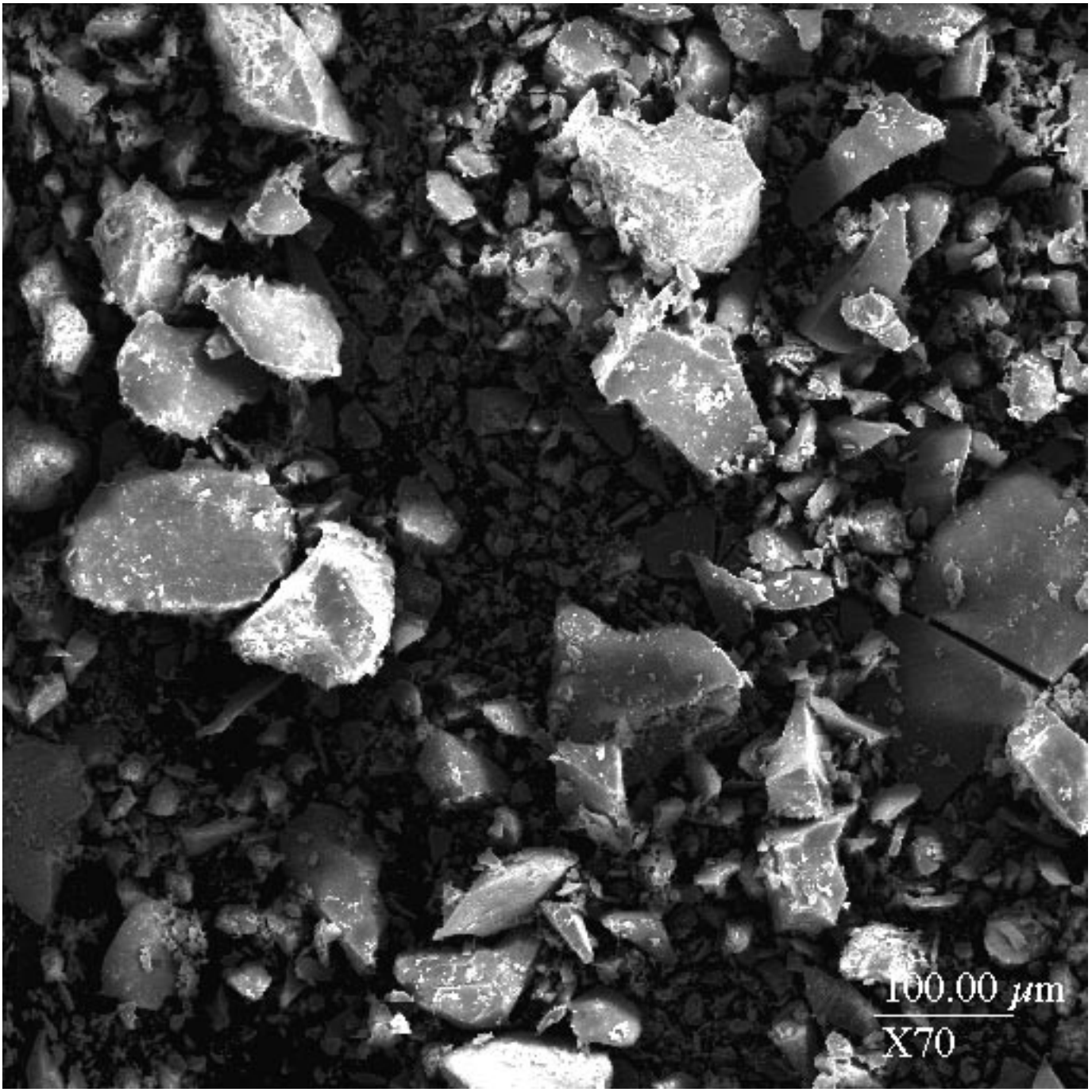

Fig. 14 Scanning Electron Micrograph of sample PRFECU-ED15-148 whose ultrasonic fragmentation results were presented on the previous page. The catalyst was prepared by Robert Gormley at FETC and is a precipitated Fe, Cu catalyst dried in vacuum at 110 °C. The catalyst is composed of irregularly shaped agglomerates. As seen from Fig. 13, these agglomerates are quite strong but they have a rather broad size distribution with a significant amount of fine particles.

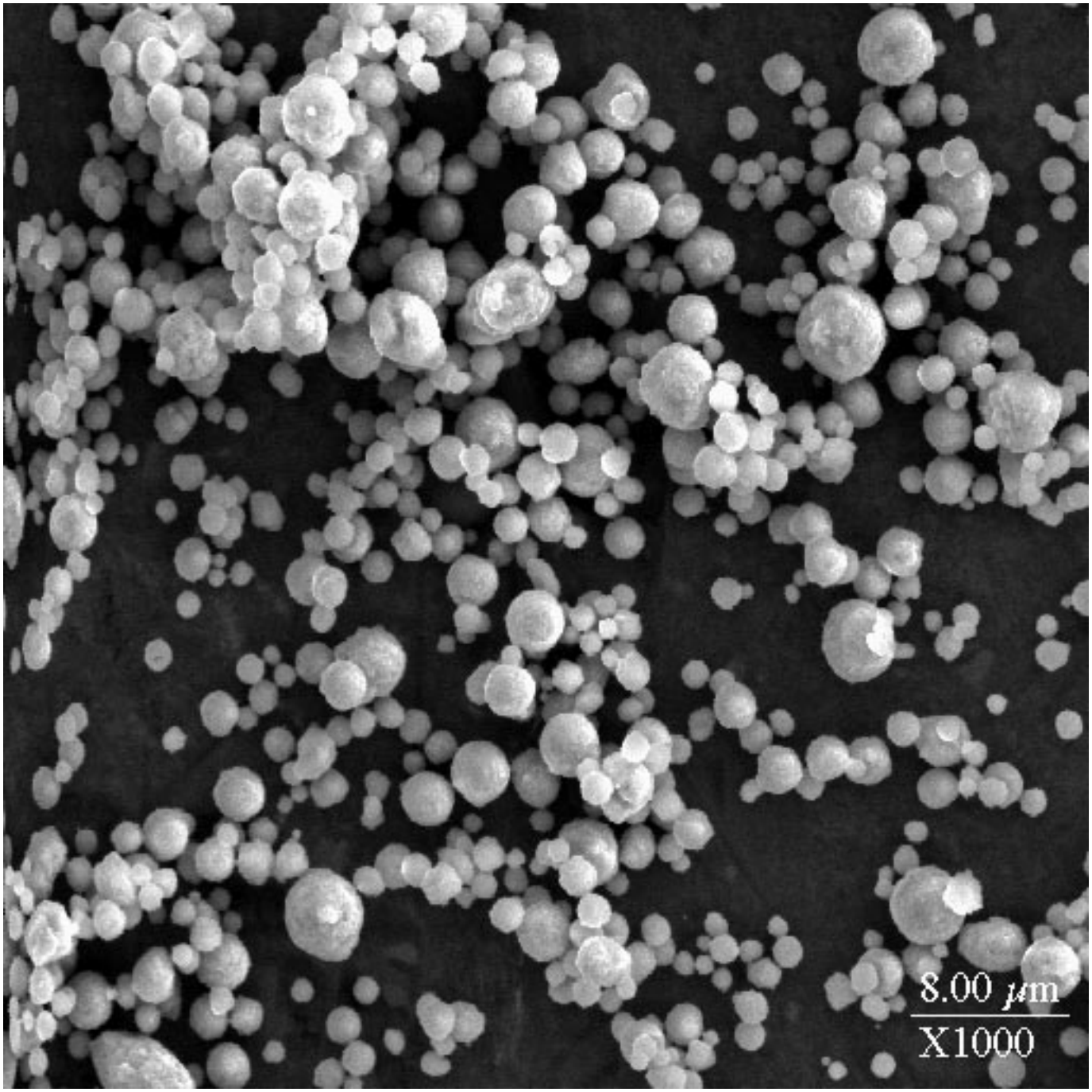

Fig. 15 Scanning Electron Micrograph of a precipitated Fe, Cu, K catalyst spray dried at UNM with a silica binder. Spherical particles typical of a spray dried powder can be seen. Ultrasonic fragmentation results on this sample are presented on the next page.

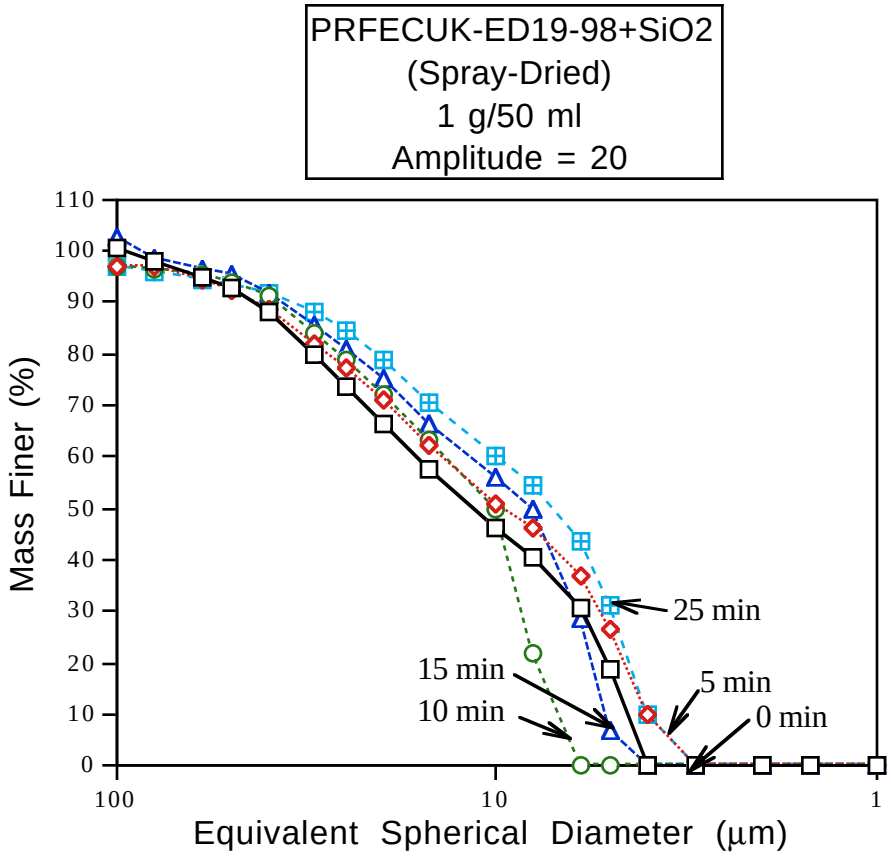

Fig. 16 Ultrasonic fragmentation results for the spray dried powder shown in Fig. 15. For comparison, fragmentation results obtained with the base case Fe catalyst (used for Laporte I) and a Vista alumina catalyst support are shown on the next page (reproduced from our Feb 1997 progress report). The spray dried Fe catalyst (shown above) appears to be comparable in strength to the alumina support (17 b).

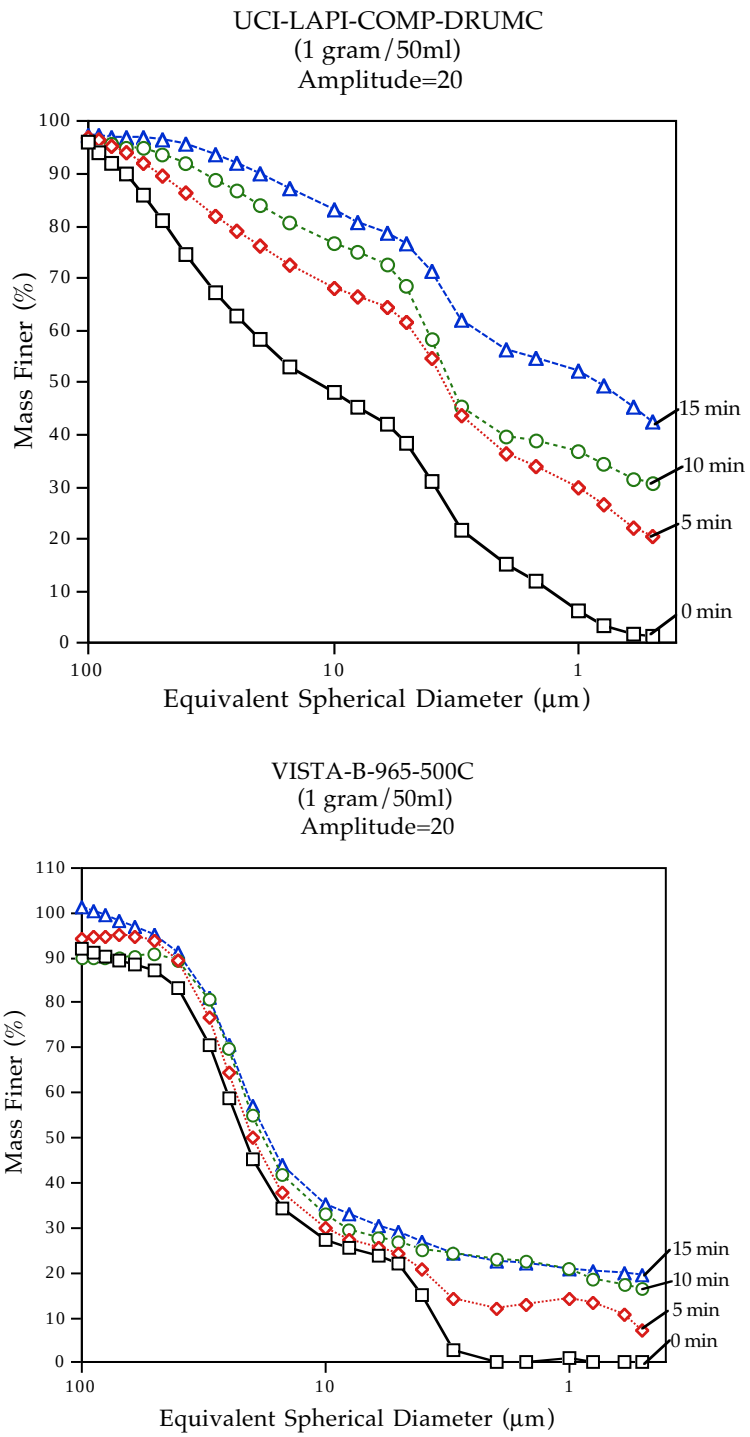

Fig. 17 Comparison of the ultrasonic fragmentation of the Fe base catalyst and a commercial alumina support. The Fe catalyst appears to break down by particle rupture as well as erosion, while erosion is the only mechanism occurring with the alumina support. Compaction tests for these two catalysts are shown in Fig. 18

18 a

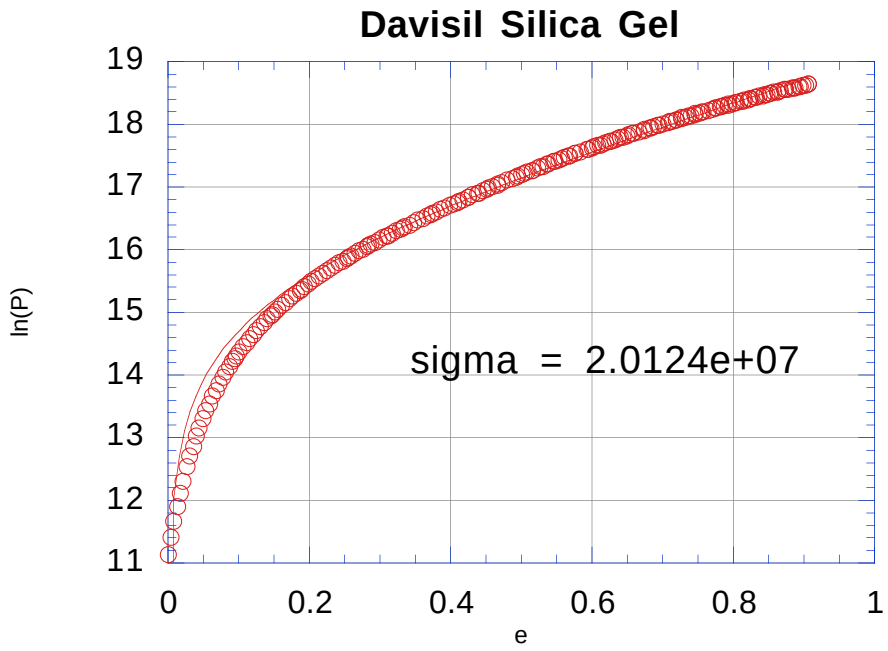

Figure 18 Compaction tests of three catalyst powders
a) Davisil silica gel (strength = 20.12 MPa)
b) Fe catalyst used for Laporte I (strength = 6.3 MPa)
c) Vista alumina support (strength = 7.4 MPa)

Davisil silica appears to have the strongest particles while the Vista alumina and the Fe catalyst are comparable. Note that the Davisil silica is not spray dried and while the strengths of the alumina and Fe catalysts are similar, their fragmentation behavior shown in Fig. 17 is very different. The Fe catalyst shows significant breakdown at energies where the alumina only exhibits mild erosion.

18 b

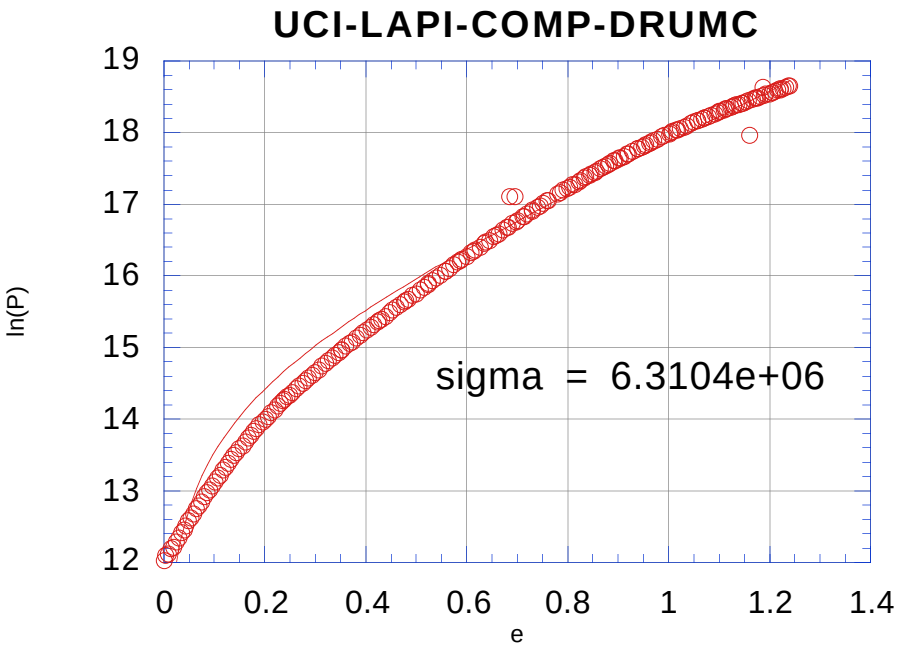
UCI-LAPI-COMP-DRUMC
ln(P)
19
18
17
16
15
14
13
12
0
0.2
0.4
0.6
0.8
1
1.2
1.4
e
sigma = 6.3104e+06

18 c

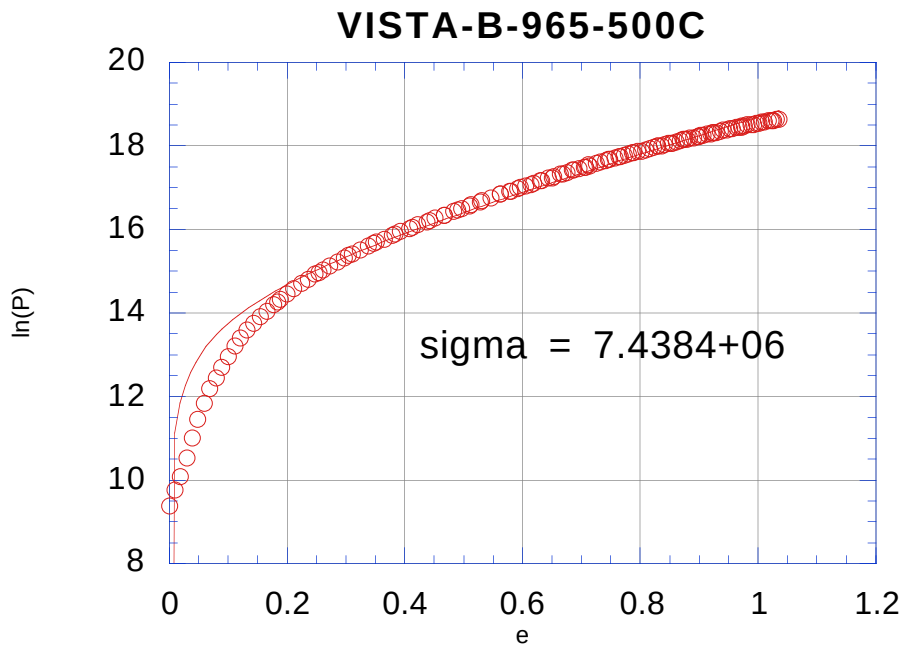
VISTA-B-965-500C
ln(P)
20
18
16
14
12
10
8
0
0.2
0.4
0.6
0.8
1
1.2
e
sigma = 7.4384+06

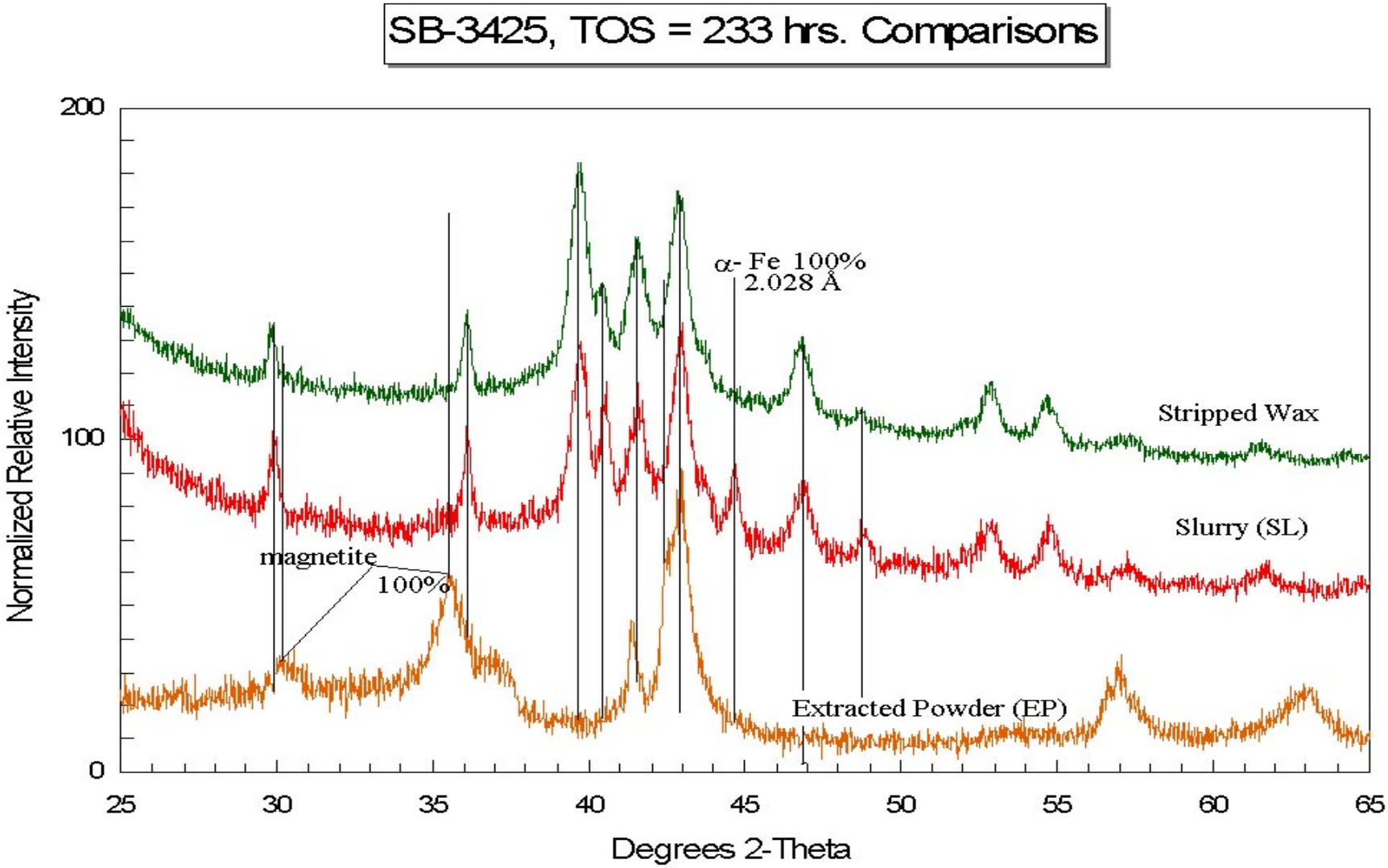

Figure 19 X-ray diffraction powder patterns of the Texas A&M catalyst as-received in the wax (slurry). Also shown is a powder pattern of this catalyst after the wax was extracted via solvent extraction. The pattern at the top comes from the wax alone, free of any catalyst. Note how the α-Fe peak in the as-received catalyst is absent in the solvent extracted sample as well as the wax (which does not contain any catalyst). The magnetite peaks in the solvent extracted sample arise due to sample oxidation and were not seen in the as-rceived sample.

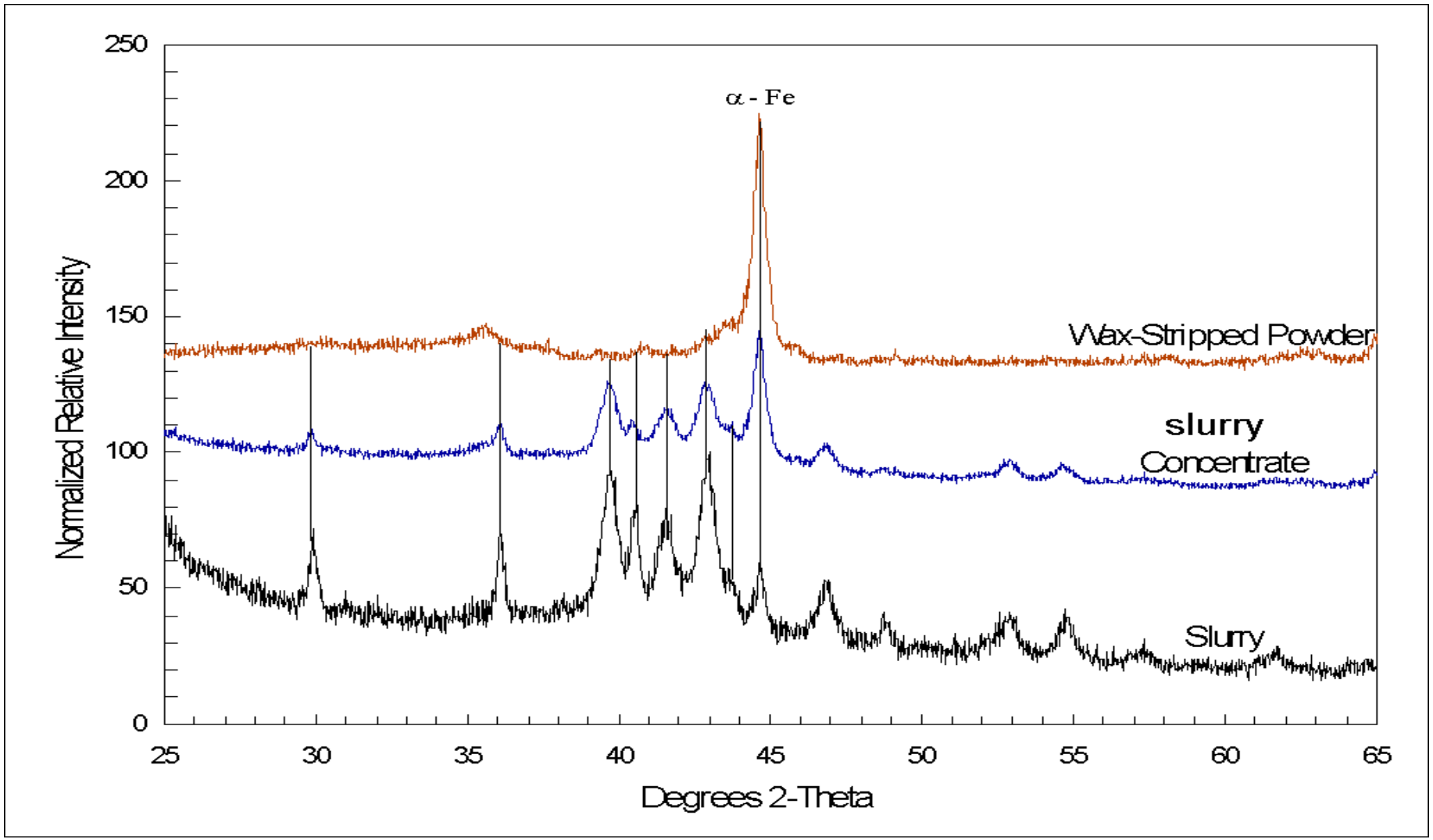

Figure 20 X-ray diffraction powder pattern of the Texas A&M catalyst as -received in wax (slurry). The catalyst loading was increased by allowing it to settle and analyzing the sediment (slurry concentrate). To eliminate peaks from the wax, this concentrate sample was heated in flowing Helium up to 400 °C to strip the wax (wax-stripped powder). The unmistakable conclusion from this series of xrd patterns is that a-Fe is a major constituent of the working catalyst this reactor (run SB-3425 time on stream 330 hours).

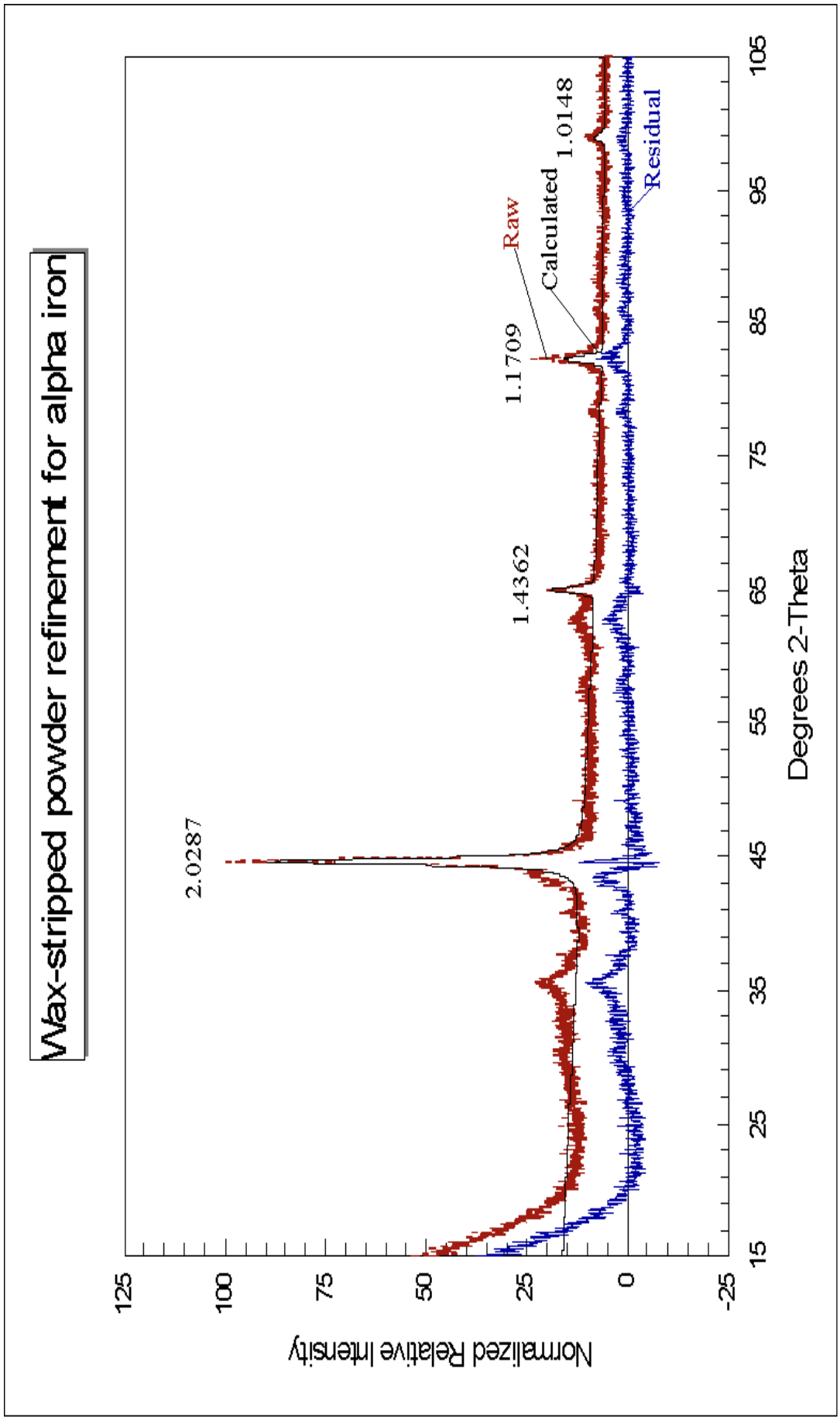

Fig. 21 Reitveld refinement of the xrd pattern of the wax stripped powder shown in Fig. 20. After subtraction of the α-Fe peak, we see some residual peaks that are shown in greater detail in the next figure. The major constituent is definitely α-Fe.

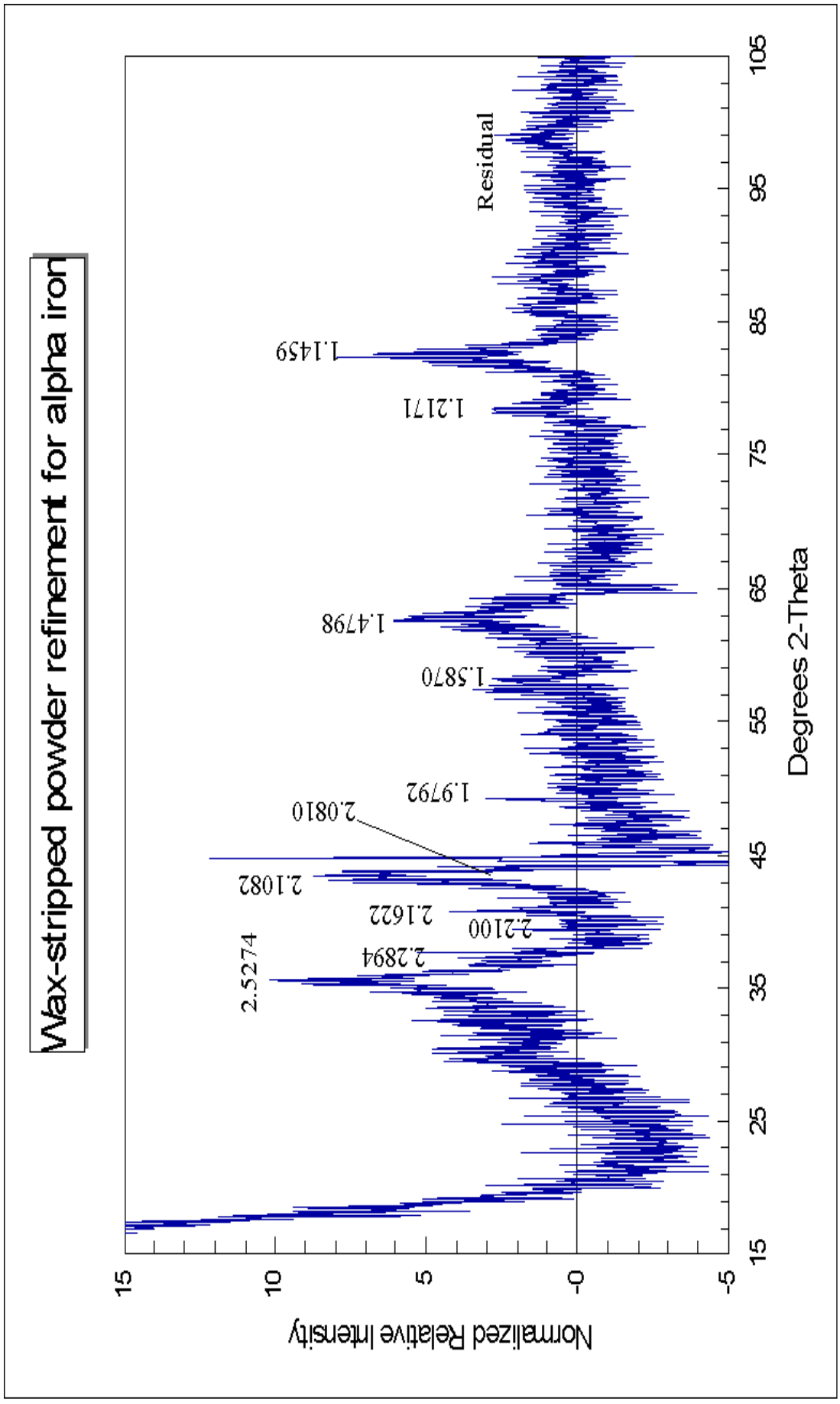

Fig. 22 The residual after subtraction of the α-Fe from the wax-stripped powder. The peak at 2.52 Å may correspond to magnetite while the other peaks may come from iron carbides.

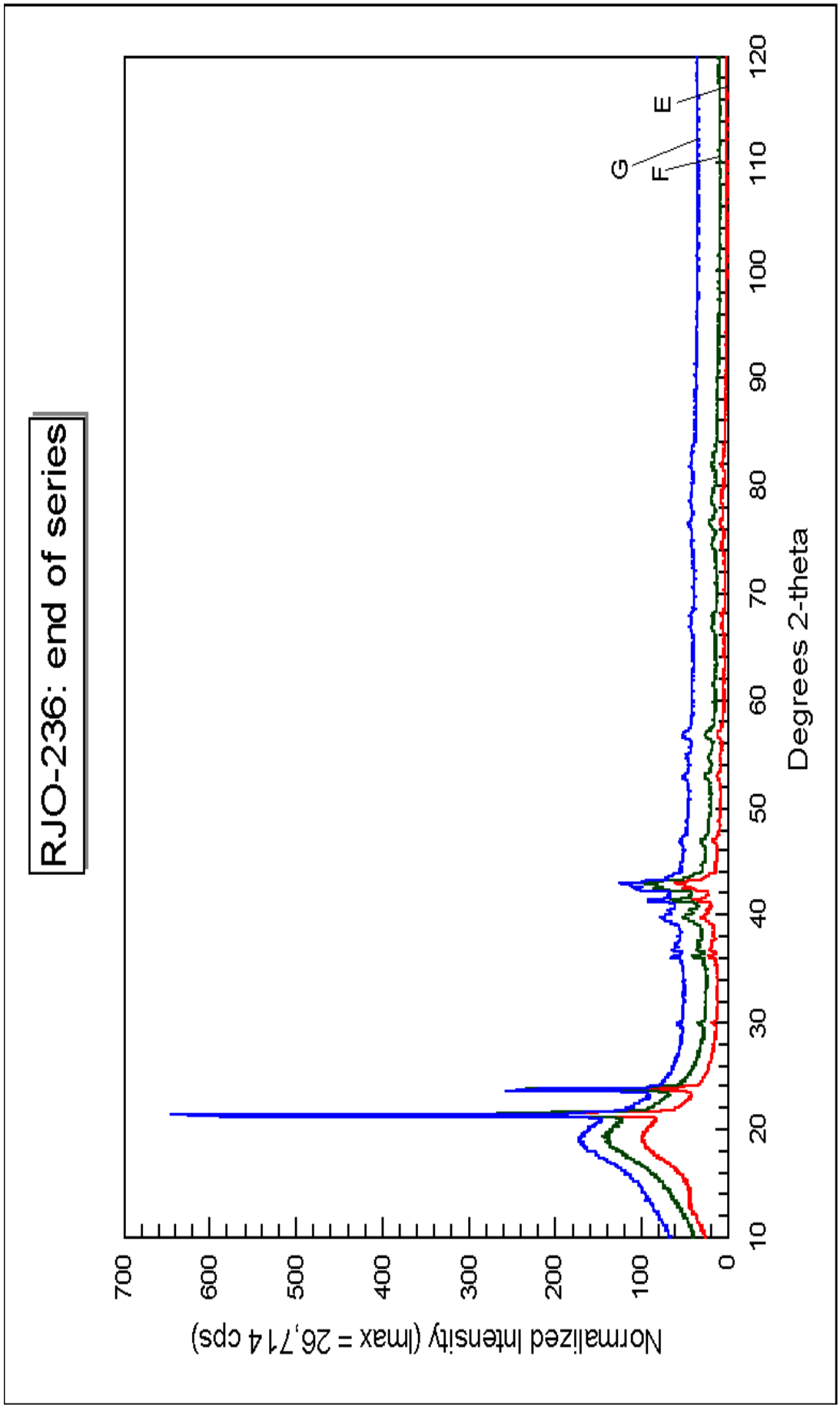

Fig. 23 X-ray diffraction pattern of samples received from CAER from a F-T run. This sample was received in the wax and had been removed under an inert blanket. An expanded view of this xrd pattern is shown in the next figure. Samples E, F and G were withdrawn at increasing time on stream during a F-T run.

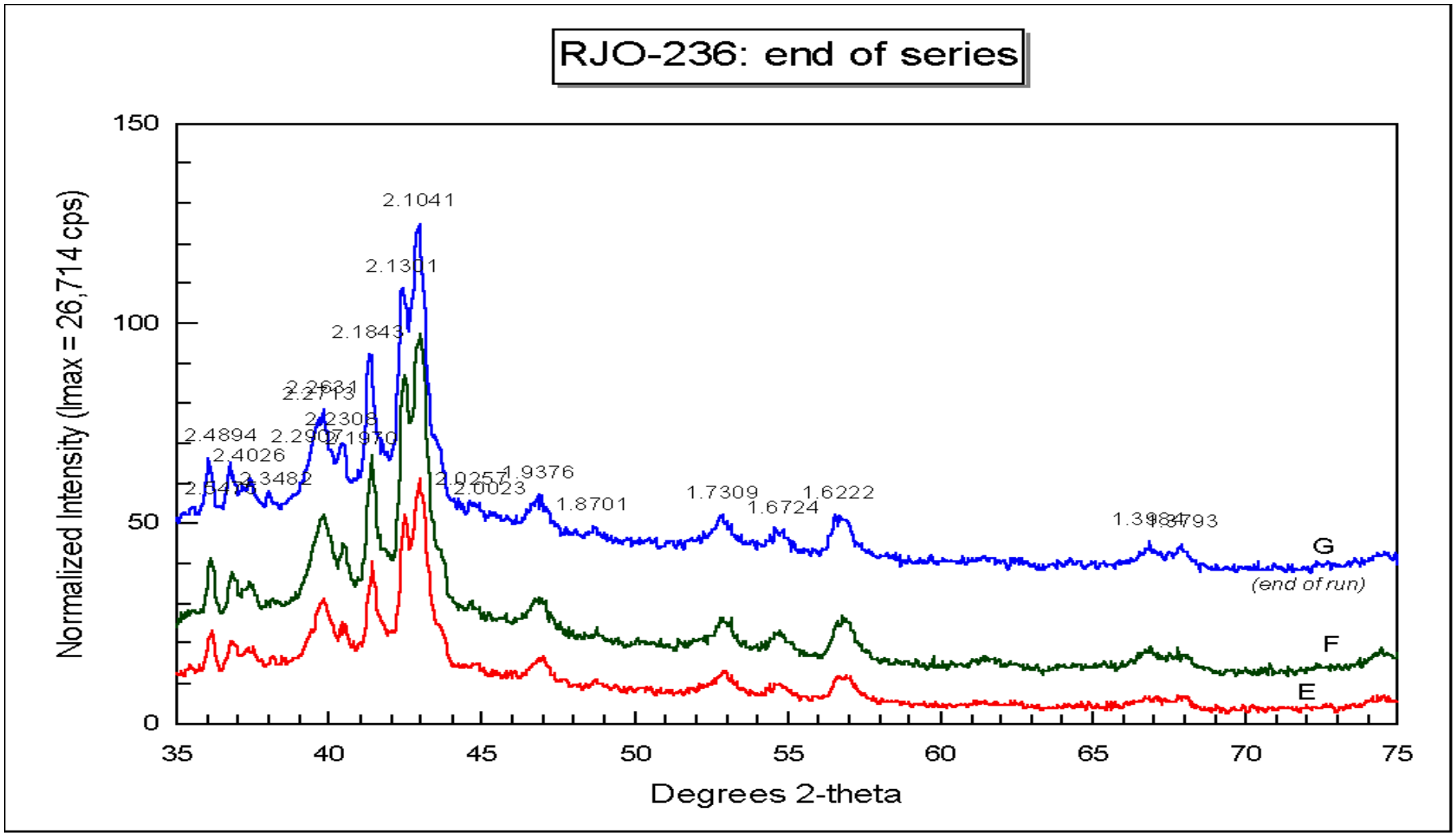

Fig. 24 An expanded view of the xrd patterns shown in Fig. 23. The peaks appear to come from iron carbide and there is no evidence for any magnetite. This result suggests that magnetite may not be present in significant amounts in an F-T slurry reactor. Removal of hot wax under inert blanket is necessary to preserve the phase composition of the working catalyst.